

## Chapter 2

# Theoretical Approaches for Multiscale Computer Simulations

**Abstract** This chapter presents a summary of main theoretical methods that are implemented in MBN EXPLORER. The significant part of the methodologies outlined is devoted to the classical molecular dynamics, which is based on the concept of molecular force fields. A variety of different force fields is introduced and their applicability to the description of molecular systems of different kind is discussed. Special attention is paid to biomolecular systems. The key algorithms (integrators, linked cell approach, Ewald summation, etc.), as well the essential aspects of the computational realisation of molecular dynamics (thermostats, boundary conditions, etc.) are elaborated in details. The basic ideas towards the multiscale description of MBN systems by means of kinetic Monte Carlo approach and the irradiation driven molecular dynamics are introduced and discussed.

### 2.1 Hierarchy of Theoretical Methods and Their Limitations: *ab initio* Methods and Model Approaches

The equations that describe the physical and chemical behaviour of real systems are often too complicated to be solved analytically, implying numerical computations. In order to save computational resources, which are typically limited, the description of real life phenomena has to be simplified. Fortunately, often not all details need be taken into account in order to reproduce and predict experimental results. Key assumptions about reality can be made ignoring the redundant complexity that is not necessary to describe the given situation, in other words to introduce the so-called models.

Convenient way of modelling meso-, bio-, nano systems consists in separating the models according to the entity whose behaviour is described (electrons, atoms, molecules, nanoparticles and grains and continuum unit cell). This philosophy is generally followed in MBN EXPLORER, as various theoretical approaches involve description of different physics or chemistry. This is often related to the time and length scale of the processes and determines the size of the systems that can be simulated with certain available computer resources. For example, diffusivity may be simulated modelling electrons diffusion, ion transport at atomistic level and electrical

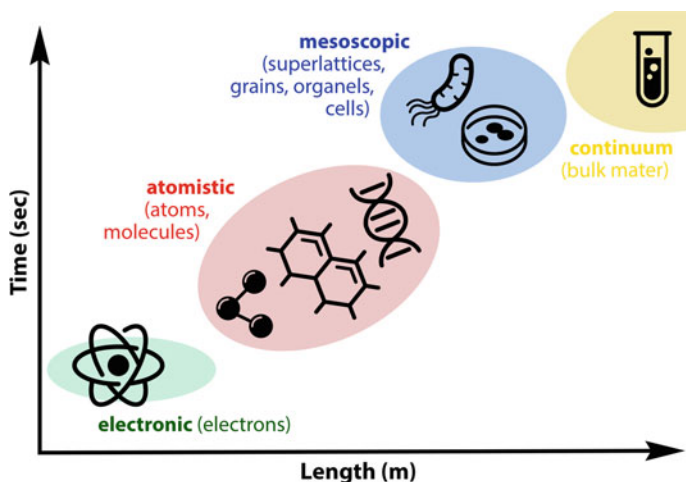


**Fig. 2.1** An illustration of entities in the different model types at different length and time scales

current with continuum models. Another example is modelling of chemical reactivity using molecular simulations at the atomistic scale and continuum reaction kinetics thereafter.

The general hierarchy of computational models is illustrated in Fig. 2.1. Although, the presented methodologies go beyond the current capabilities of MBN EXPLORER, they summarize the main theoretical methods ranging from electronic and atomistic ab initio techniques (below called models) to those at the bulk limit. Thus, the available computational models in MBN science can naturally be subdivided into:

**Electronic models:** These models describe behaviour of electrons. Methods of quantum mechanics (QM) are used to describe the behavior of the electrons which determine the properties and structures of the material. Ab initio models calculate electronic structures “from first principles” (i.e. based on fundamental principles of physics) expressed in the Schrödinger’s equation within a set of approximations that do not include fitting the model to experimental data. These models thus rely on basic and established laws of nature without ad hoc parameterisation. Here, the material is explicitly represented by nuclei and electrons. From the model results at these shortest atomic time/length scales, electronic transitions and chemical reactions can be derived. More examples include: electronic band structure, conductive/dielectric and optical properties, force fields parameters, (magnetic) anisotropy, diffusion coefficient, activation energies, thermodynamic stability and kinetic elementary processes for atomic defects and dopants. The current version of MBN EXPLORER does not support electronic structure calculation, but could readily be coupled with outputs of the well established quantum chemistry software, e.g. Gaussian [97].

**Atomistic models:** These models describe the behaviour of atoms. When the electronic degrees of freedom are ignored, molecular mechanical (MM) models and classical mechanics are applied to describe the behavior of atoms and molecules.

In addition to quantum mechanics based techniques, atomistic modelling uses effective interactions between atoms, called interatomic potentials (also empirical potentials or force fields). Interatomic potentials do not treat the quantum nature of electrons explicitly, which allows models using these potentials to be enormously faster than models using quantum methods. Such interatomic potential based modelling may not be as accurate as full quantum mechanical approaches, but can be used to simulate complex materials processes as radiation damage in nanocrystalline materials and friction between surfaces. The most common technique here is molecular dynamics (MD) simulations, now routinely carried out on systems including up to tens of thousands of molecules (consisting of many atoms) over tens of nano seconds. At these longer time scales e.g. lattice motion is described. Further examples include: atomic trajectories, packing, stiffness, dynamical properties, surface and interface energies, constitutive equations parameters, spectral properties. The theoretical foundations of atomistic simulations in MBN EXPLORER are described in the following sections of this chapter.

**Mesoscopic models:** These models describe, for example, the behavior of nanoparticles or grains. At the supra-atomic scale where uninteresting or fast details of the atomic motions are averaged out or replaced by stochastic terms, mesoscopic models concentrate on essential motions and large-scale structures. Examples are thermodynamics models. Also the so-called coarse-grained models fall in this category and here the fundamental unit is a “bead” that interacts with other “beads” via effective soft potentials. This category of models also includes the magnetism models based on macro-spin approaches that combine atomic spins into a macro-spin. Examples of mesoscopic model results: morphology, domain formation and growth kinetics, thermal stability, magnetic behaviour. Mesoscopic models are often relying on kinetic Monte-Carlo simulations, and are possible through MBN EXPLORER, as detailed in Sect. 2.5 of this chapter.

**Continuum models:** These models describe the behavior of a continuum unit cell. At this level material is assumed to be continuously distributed throughout its volume. Models at this scale disregard the discrete particle-based structures and smaller detail. This level describes how materials are seen and touched. Modelling at this scale can predict material decomposition, defect formation, crack propagation, solidification of liquids and other important variables for industrial manufacturing. At these macroscopic length scales e.g. thin films and realistic nano-devices with metallic contacts are described. Examples for macroscopic model results in macroscopic structural behaviour, heat and mass transport, permeation times, chemical reaction kinetics, electromagnetic behaviour.

In order to increase their predictive capability and applicability to a wide range of applications, continuum-scale models need to include processes, which originate at the electronic, atomistic and nanoparticle-scale. Often, in the continuum-scale models such effects are neglected. For example, continuum-scale models that approximate interfaces by a set of effective band offset parameters have no predictive power over interface related effects as the detailed electronic and atomistic structure near the interfaces is not taken into account. Thus, it is a great challenge in creating accurate and predictive models accounting for the true multi-scale nature of materials.

A consistent hierarchy of simulations at different levels of representation dealing with different segments of the physics/chemistry is needed. These simulations should be linked into a single multi-scaling scenario describing the behaviour of the entire system. In this respect, MBN EXPLORER is a unique software as it links different types of models (methodologies for simulation) for atoms, molecules, nanoparticles, mesoscopic and continuum systems within one computational package. This chapter overviews the essential theory of the conventional and multiscale methods implemented in the program.

## 2.2 Methods for Studying Dynamical Molecular Processes and Related Phenomena

Different methods for studying dynamical processes in MBN EXPLORER allows simulations of different physical systems and phenomena. The program is designed in a multiscale fashion, such that different types of calculations can inter-rely on each another and use the output from one calculation at a next scale. All methods currently implemented in the program can be categorized in seven areas such as

- single-point energy calculation;
- structure optimisation;
- molecular dynamics;
- Euler dynamics;
- irradiation driven molecular dynamics;
- random walk dynamics;
- relativistic dynamics.

**Single-point energy calculation** allow establishing the total energy of a given molecular system. In this case the interaction between atoms is defined through parametrisation of the potential energy. Different potentials including pairwise (Lennard-Jones, Morse, Dzugutov, Girifalco, Power, Exponential, quasi Sutton-Chen, and Coulomb), many-body potentials (Sutton-Chen, Gupta, Brenner, Tersoff, Finnis-Sinclair), and potentials for molecular mechanics could be used to model different physical systems. The details of the listed potentials are summarized below in this chapter.

**Structure optimisation** algorithms permit to establish a configuration of a molecular system that corresponds to a local or a global minimum on a multidimensional potential energy landscape. Two algorithms of minimization currently implemented in MBN EXPLORER are the velocity quenching (VQ) and conjugate gradient [98], which can be used for any type of interatomic interactions permitted by the software. Structure optimisation is a typical and necessary step that has to be completed prior any dynamical studies, as those often need to be carried out from an equilibrium configuration of a molecular system.

**Molecular dynamics** collects the core algorithms and methods that are used to study different kinds of dynamical transformations in MBN systems. MBN

EXPLORER supports Newtonian, Euler and Langevin dynamics, and the details of the underlying algorithms are discussed below.

**Euler dynamics** describes dynamics of a system of rigid bodies, which could be represented by a set of interacting molecular systems with the frozen internal degrees of freedom.

**Irradiation driven molecular dynamics** a new type of multiscale MD allowing one to account for the irradiation driven molecular transformations on molecular systems caused by their irradiation.

**Random walk dynamics** allows simulations of diffusion-driven processes in different systems with the MC algorithm.

**Relativistic dynamics** permits simulations of scattering and channeling of the relativistic particles in various systems.

Below we outline the basic concepts of the key methods implemented in MBN EXPLORER.

### 2.2.1 Newtonian Dynamics

Newton's equations describe the classical motion of atoms. Euler's equations are employed to describe the motion of rigid molecules. In the latter case one has to account for the spatial rotation of molecules by introducing three additional rotational degrees of freedom per molecule.

The Newton's equations of motion for all atoms in the system read as:

$$m_i \mathbf{a}_i = m_i \frac{d^2 \mathbf{r}_i}{dt^2} = \mathbf{F}_i, \quad i = 1, \dots, N_{\text{at}}. \quad (2.1)$$

Here  $m_i$  is the mass of an atom,  $\mathbf{a}_i$  is its acceleration and  $\mathbf{F}_i$  is the force that acts on the atom, and  $N_{\text{at}}$  is the total number of atoms in the system which are not constrained within rigid molecules. The forces  $\mathbf{F}_i$  are determined by the interatomic potentials and external force fields. These forces may be pairwise, or many-body in nature. To solve Eq. (2.1) numerically one needs to provide initial conditions, i.e., define initial positions and velocities of particles at time instance  $t = 0$ .

### 2.2.2 Relativistic Dynamics

In cases when relativistic effects become important, the equations of particle motion have to be modified to account for such effects. For each relativistic particle, i.e. projectile particle, MBN EXPLORER is thus required to solve the corresponding relativistic equation of motion, which read as:

$$\begin{cases} \dot{\mathbf{v}} = \frac{1}{m\gamma} \left( \mathbf{F} - \mathbf{v} \frac{\mathbf{F} \cdot \mathbf{v}}{c^2} \right) \\ \dot{\mathbf{r}} = \mathbf{v} \end{cases}, \quad (2.2)$$

where  $\gamma = \varepsilon/mc^2 = (1 - v^2/c^2)^{-1/2}$  stands for the so-called relativistic Lorentz factor with  $\varepsilon$  and  $m$  being the projectile energy and mass, respectively. The force  $\mathbf{F} = -\nabla U(\mathbf{r})$  acting on the projectile is due to its interaction with the surrounding atoms. In Sect. 9.4 we discuss the possible choice of this interaction in application to real physical systems.

### 2.2.3 Rigid Body Dynamics

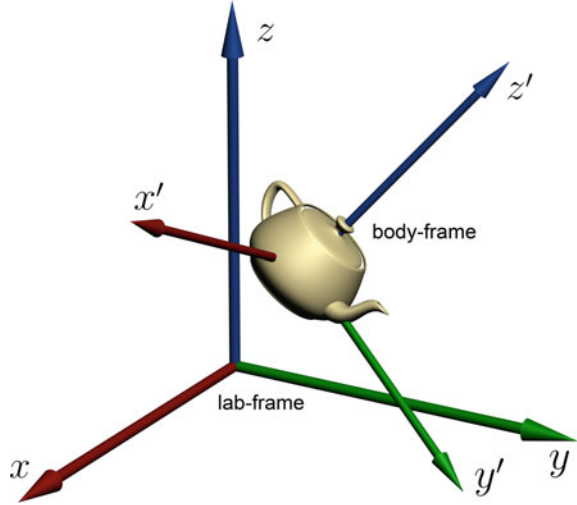
Rigid body molecular dynamics deals with the motion of rigid molecules (or their parts), in which distances between any two atoms within the rigid fragment are fixed. In a fixed reference frame (called the lab-frame), the location and orientation of the molecule is described through (i) motion of the center of mass of the molecule with respect to the origin of the lab-frame; (ii) orientation of the molecule with respect to the lab-frame. Therefore, the position and the orientation of a rigid molecule can be defined with 3 spatial and 3 angular variables. Thus, the equations describing the motion of a rigid molecule are the Newton equations, Eq. (2.1), for the motion of the center of mass and the Euler equations for its rotation. The rotational motion is governed by the following equations [99]:

$$\frac{d\mathbf{L}_\alpha}{dt} = \mathbf{T}_\alpha, \quad \alpha = 1, \dots, N_{\text{rm}}. \quad (2.3)$$

Here  $\mathbf{L}_\alpha$  is the total angular momentum of a rigid molecule with respect to the origin of the lab-frame,  $\mathbf{T}_\alpha$  is its total torque, and  $N_{\text{rm}}$  is the total number of rigid molecules in the system. Equation (2.3) describes the evolution of the angular momentum of a rigid molecule with time under the action of external torques. This equation is only valid in an inertial frame. However, the frame in which the coordinate axes are aligned along the principal axes of rotation of the molecule and  $\mathbf{L}_\alpha$  possesses its simplest form is non-inertial. Thus, it is helpful to define two Cartesian coordinate systems: the first one with coordinates  $(x, y, z)$ , is the fixed lab-frame, while the second molecular-frame, with coordinates  $(x', y', z')$ , co-rotates with the molecule so that the  $x'$ -,  $y'$ -, and  $z'$ -axes are always pointing along the principal axes of rotation, see Fig. 2.2. Since the molecular-frame co-rotates with the molecule, its instantaneous angular velocity coincides with that of the molecule. Hence,

$$\frac{d\mathbf{L}_\alpha}{dt} = \frac{d\mathbf{L}'_\alpha}{dt} + \boldsymbol{\omega}'_\alpha \times \mathbf{L}'_\alpha. \quad (2.4)$$

**Fig. 2.2** Two coordinate frames used to describe the motion of a rigid molecular object:  $(x, y, z)$  represents the fixed laboratory frame, while the non-inertial coordinate frame  $(x', y', \text{and } z')$  is the object frame, in which its tensor of inertia is diagonal



Here,  $\boldsymbol{\omega}'_{\alpha}$  and  $\mathbf{L}'_{\alpha}$  are the angular velocity and the angular momentum of a rigid molecule in the molecular-frame. Introducing the Cartesian components of the vectors  $\mathbf{T}'_{\alpha} \equiv (T'_{\alpha_{x'}}, T'_{\alpha_{y'}}, T'_{\alpha_{z'}})$ ,  $\boldsymbol{\omega}'_{\alpha} \equiv (\omega_{\alpha_{x'}}, \omega_{\alpha_{y'}}, \omega_{\alpha_{z'}})$ , and  $\mathbf{L}'_{\alpha} \equiv (I_{\alpha_{x'x'}}\omega_{\alpha_{x'}}, I_{\alpha_{y'y'}}\omega_{\alpha_{y'}}, I_{\alpha_{z'z'}}\omega_{\alpha_{z'}})$ , where  $I_{\alpha_{x'x'}}$ ,  $I_{\alpha_{y'y'}}$  and  $I_{\alpha_{z'z'}}$  are the principal moments of inertia of the molecule, one writes the components of Eq.(2.3) as

$$T_{\alpha_{x'}} = I_{\alpha_{x'x'}} \dot{\omega}_{\alpha_{x'}} - (I_{\alpha_{y'y'}} - I_{\alpha_{z'z'}}) \omega_{\alpha_{y'}} \omega_{\alpha_{z'}}, \quad (2.5)$$

where  $(x', y', z')$  undergo cyclic permutations. Here we have used the fact that moments of inertia of a rigid molecule are constant in time in the co-rotating molecular-frame.

### 2.2.4 Temperature Control

According to the equipartition theorem [100], every degree of freedom in the system,  $f$ , has the same kinetic energy,  $\langle \mathcal{H} \rangle_f = k_B T/2$ . Therefore, the effective temperature  $T$  of the system is given by the ensemble average of its kinetic energy:

$$T = \frac{2}{gk_B} \left\langle \sum_{f=1}^g \mathcal{H}_f \right\rangle = \frac{1}{3(N_{\text{at}} + 2N_{\text{rm}})k_B} \left\langle \sum_{i=1}^{N_{\text{at}}+N_{\text{rm}}} m_i \mathbf{v}_i^2 + \sum_{i=1}^{N_{\text{rm}}} \boldsymbol{\omega}_i \cdot \hat{I}_i \cdot \boldsymbol{\omega}_i \right\rangle. \quad (2.6)$$

Here  $g = 3N_{\text{at}} + 6N_{\text{rm}}$  is the number of degrees of freedom,  $N_{\text{at}}$  is the number of atoms having three degrees of freedom and  $N_{\text{rm}}$  is the number of rigid molecules with six degrees of freedom. It is often desirable that a simulation is conducted in

a way that the temperature is kept constant. This requires some mechanism to fix the average kinetic energy at thermal equilibrium. MBN EXPLORER offers several techniques for temperature control. The common technique of velocity scaling (the Berendsen thermostat) is suitable for use during the equilibration period of a simulation, while the Langevin dynamics describes the evolution of a molecular system which experiences random collisions with “virtual” particles that mimic environment (the Langevin thermostat).

A simple velocity scaling thermostat is that of Berendsen et al. which is referred to as the Berendsen thermostat in literature [101]. At periodic intervals linear and angular velocities of all particles in the system are multiplied by a constant factor

$$\lambda = \sqrt{1 + \frac{\Delta t}{\tau_T} \left( \frac{T}{T_0} - 1 \right)}. \quad (2.7)$$

Here,  $T_0$  is the thermostat temperature,  $T$  is the temperature of the system, and  $\Delta t$  is the integration time step. The parameter  $\tau_T$ , called the “rise time” of the thermostat, characterises the strength of system’s coupling to a virtual heat bath. Larger values of  $\tau_T$  correspond to weaker coupling; in other words, the larger  $\tau_T$  is, the longer it takes for a system to achieve a given  $T_0$ . By repeatedly setting the “instantaneous” temperature to a given value during the simulation, the average kinetic energy is made to approach a constant value.

In the Langevin dynamics, atoms in the system are considered to be embedded in a “sea” of fictional particles. In this case, the dynamics of atoms in the system is described by the Langevin equations of motion which include additional terms accounting for the friction force and for the noise:

$$m_i \frac{d^2 \mathbf{r}_i}{dt^2} = \mathbf{F}_i - \frac{1}{\tau_d} m_i \mathbf{v}_i + \sqrt{\frac{2k_B T_0 m_i}{\tau_d}} \mathbf{R}_i(t), \quad i = 1 \dots N_{\text{at}}. \quad (2.8)$$

Here  $\mathbf{F}_i$  is the physical force acting on the atom,  $k_B T$  denotes the thermal energy in the system,  $\tau_d$  is the characteristic viscous damping time, and  $\mathbf{R}_i(t)$  represents a delta-correlated stationary Gaussian process with zero-mean, satisfying

$$\langle \mathbf{R}_i(t) \rangle = 0, \quad \langle \mathbf{R}_i(t) \mathbf{R}_i(t') \rangle = \delta(t - t'), \quad (2.9)$$

where  $\langle \dots \rangle$  denotes time-averaging.

The Langevin equation of motion, Eq. (2.8), gives a physically correct description of a many-particle system interacting with a heat bath, maintained at a constant temperature  $T_0$ . The viscous damping time parameter,  $\tau_d$ , describes the characteristic time of energy exchange between particles and the heat bath. This parameter should be chosen carefully. If  $\tau_d$  is small, the Brownian dynamics tends to dominate over the Newtonian dynamics of the system, potentially leading to physically wrong results. In the opposite limit, when  $\tau_d$  is chosen to be large, the system requires a long period to attain the desired temperature.



It is straightforward to couple the rigid molecule equations of motion to a thermostat. The thermostat is coupled to both the translational and rotational degrees of freedom and so both the translational and angular velocities can be treated similarly. The Langevin dynamics of the translational degrees of freedom of a rigid molecule obeys Eq. (2.8). Interaction of rigid molecules with the environment introduces two additional terms in the Euler equation (2.5) which modify the torque acting on the molecule:

$$\mathbf{T}_\alpha = \mathbf{T}_{0_\alpha} - \frac{1}{\tau_d} \hat{I}'_\alpha \boldsymbol{\omega}'_\alpha + \sqrt{\frac{2k_B T_0 \hat{I}'_\alpha}{\tau_d}} \mathbf{R}'_\alpha(t), \quad i = 1 \dots N_{\text{rm}}. \quad (2.10)$$

Here  $\mathbf{T}_{0_\alpha}$  is the torque acting on the rigid molecule according to Eq. (2.3),  $\boldsymbol{\omega}'_\alpha$  is the angular velocity of a rigid molecule,  $\hat{I}'_\alpha$  is the diagonalized tensor of moments of inertia and  $\mathbf{R}'_\alpha(t)$  represents a delta-correlated stationary Gaussian process with zero-mean, satisfying conditions (2.9).

Berendsen and Langevin thermostats provide for the basic functionality to control the temperature of the system. For systems composed of particles with three degrees of freedom, these thermostats are rather standard and are also available in most computational packages [30, 32, 33, 35, 39]. The thermostats implemented in MBN EXPLORER allow generalization for systems comprising rigid molecules (having six degrees of freedom).

Note, that it is important to choose thermostat appropriately depending on the physical problem to be solved. The Langevin equation (2.8) puts constraints on the random forces and the friction applied to the particles in the system such that the random force and the friction terms become related, thereby satisfying the fluctuation-dissipation theorem and guaranteeing the NVT statistics. Figure 2.3a shows distribution of temperature fluctuations computed for a  $\text{C}_{60}$  molecule subject to the Langevin thermal bath; the data points were sampled from a 1 ns long MD simulation at 300 K. To compute the distribution shown in Fig. 2.3a, the following procedure was employed: during the simulation, the immediate value of temperature of  $\text{C}_{60}$  molecule was stored on every step of the simulation. Next, the recorded temperatures were sorted in bins of 10 K width and plotted in a form of a distribution function. The computed distribution can be compared with the fundamental distribution of temperature fluctuations [100], having the form

$$p(\Delta T) = \frac{1}{\sqrt{2\pi}\sigma} \exp\left(-\frac{(\Delta T)^2}{2\sigma^2}\right). \quad (2.11)$$

Here  $\Delta T = T - T_0$  is the deviation of the system temperature  $T$  from that of the thermostat,  $T_0$ , and  $\sigma^2 = 2T_0^2/g$  defines the width of the distribution through the number of degrees of freedom in the system,  $g$ . For a finite system consisting of particles with only three degrees of freedom,  $g = 3N$ , where  $N$  is the number of

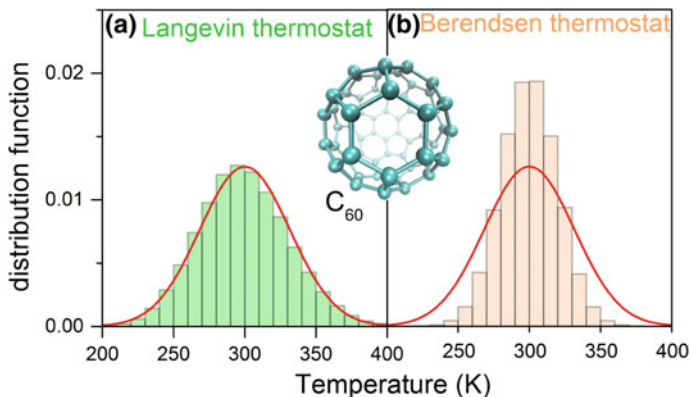


**Fig. 2.3** Distribution of temperature fluctuations computed for a  $C_{60}$  molecule (shown in the inset) subject to a Langevin thermostat (a) and Berendsen thermostat (b) during a 1 ns long MD simulation at 300 K. The parameter  $\tau_d$  of the Langevin thermostat, see Eq. (2.8), and the parameter  $\tau_T$  of the Berendsen thermostat, see Eq. (2.7), were set equal to 100 fs. The solid lines show the profile of the NVT canonical temperature fluctuations distribution computed using Eq. (2.11)

particles in the system. Figure 2.3a compares the results of the numerical simulations (the histogram) carried out with the Langevin thermostat with the fundamental distribution Eq. (2.11) where the parameters  $T_0 = 300$  K,  $N = 60$  are used (the solid curve). It is seen that the Langevin thermostat correctly describes the NVT canonical ensemble.

Contrary to the Langevin thermostat, the Berendsen thermostat fails to reproduce the distribution function (2.11), as it is illustrated by Fig. 2.3b where the histogram represents the numerical simulations of temperature fluctuations in  $C_{60}$  equilibrated using the Berendsen thermostat. Since the canonical distribution can not be reproduced, the Berendsen thermostat is not commonly used for long-run MD simulations. However, an advantage of the Berendsen thermostat is that it provides a faster equilibration of a molecular system, which is typically necessary to carry out prior any production MD simulation.

The present version of MBN EXPLORER provides two basic thermostats which are sufficient to mimic the effects of the thermal bath in the majority of computational tasks. Addition of alternative thermostats, e.g. Lowe-Andersen [102] or Nosé-Hoover thermostat [103, 104] is planned for the next releases of the software and will be documented on the MBN EXPLORER website (<http://www.mbnexplorer.com>) as soon as available. We note that the Lowe-Andersen thermostat, for example, may be important for specific problems such as the study of diffusive effects in molecular systems and environments. In this case it is important to conserve the momentum transfer in the system, that is being destroyed in the stochastic Langevin thermostat.

## 2.3 Modeling Interatomic Interactions

The potential energy functions and their derivatives determine the interatomic interactions in the system. By choosing relevant interatomic potentials MBN EXPLORER allows modelling a broad variety of molecular systems and processes with their involvement. This section discusses the interatomic interactions which are implemented in the program. It provides an overview of the potential energy functions, and discusses the parameters used to define these functions. In particular, Sect. 2.3.1 discusses pairwise potentials, while Sect. 2.3.2 is devoted to many-body potentials.

### 2.3.1 Pairwise Potentials

The total energy of the system of  $N$  particles (atoms) interacting via the pairwise potentials can be written as

$$U_{\text{tot}} = \sum_{i=1}^N \sum_{j<i}^N U(r_{ij}). \quad (2.12)$$

Here  $U(r_{ij})$  is the interaction energy of atoms with indices  $i$  and  $j$  dependent on the distance  $r_{ij} = |\mathbf{r}_i - \mathbf{r}_j|$  between the atoms.

The force  $\mathbf{F}_i$  acting on the  $i$ th particle can be calculated according to the rule:

$$\mathbf{F}_i = -\frac{\partial}{\partial \mathbf{r}_i} U_{\text{tot}} = -\sum_{\substack{j=1 \\ j \neq i}}^N \frac{\partial U(r_{ij})}{\partial r_{ij}} \mathbf{n}_{ij} \quad (2.13)$$

where  $\mathbf{n}_{ij} = \mathbf{r}_{ij}/r_{ij}$  is the unit vector along  $\mathbf{r}_{ij}$ .

Below in this section, a brief description is given of the pairwise potentials implemented in MBN EXPLORER. For the sake of reference, we present the dependencies of the potentials on interatomic distance and discuss the parameters entering the formulae for the potentials.

#### 2.3.1.1 The Power Potential

In its general form, the power potential is written as follows:

$$U(r_{ij}) = C \left( \frac{r_0}{r_{ij}} \right)^n, \quad (2.14)$$

where  $n$  is an arbitrary integer, the parameters  $C$  and  $r_0$  are measured in units of energy and length, respectively.

The power potential can be used as a ‘building block’ to construct more complicated potentials, as MBN EXPLORER allows to specify several pairwise potentials for a given pair of atoms. For example, by combining two power potentials with  $n = 12$  and  $n = 6$  one constructs the Lennard-Jones potential discussed below in the section.

### 2.3.1.2 Exponential Potential

The general form of the Exponential potential is as follows:

$$U(r_{ij}) = A \exp(-\alpha r_{ij}), \quad (2.15)$$

where the parameters  $A$  and  $\alpha$  are measured in units of energy and inverse length, respectively.

The exponential potential is another ‘building block’ among the potentials implemented in MBN EXPLORER. It can be used, for example, to construct the Morse potential through the sum of two exponents.

### 2.3.1.3 Coulomb Potential

The electrostatic interaction between two atoms with net charges  $q_i$  and  $q_j$  in the medium with dielectric permittivity  $\varepsilon$  is described in terms of the Coulomb potential:

$$U(r_{ij}) = \frac{q_i q_j}{\varepsilon r_{ij}}. \quad (2.16)$$

### 2.3.1.4 Lennard-Jones Potential

The Lennard-Jones potential is a mathematically simple model that describes the interaction between a pair of neutral atoms or molecules (van der Waals interaction) [105]:

$$U(r_{ij}) = \varepsilon \left[ \left( \frac{r_{\min}}{r_{ij}} \right)^{12} - 2 \left( \frac{r_{\min}}{r_{ij}} \right)^6 \right]. \quad (2.17)$$

The attractive long-range term,  $\propto -1/r^6$ , is due to mutual polarization of the interacting atoms. The indicated form of the repulsion term,  $\propto 1/r^{12}$ , has no theoretical justification; the repulsion force should grow exponentially at the small distances, but the repulsion term in the Lennard-Jones formula grows according to the power law, which is more convenient from the computational point of view. Its physical origin is related to the Pauli principle: when the electronic clouds of the atoms start to overlap, the energy of the system increases abruptly due to the exchange interaction.

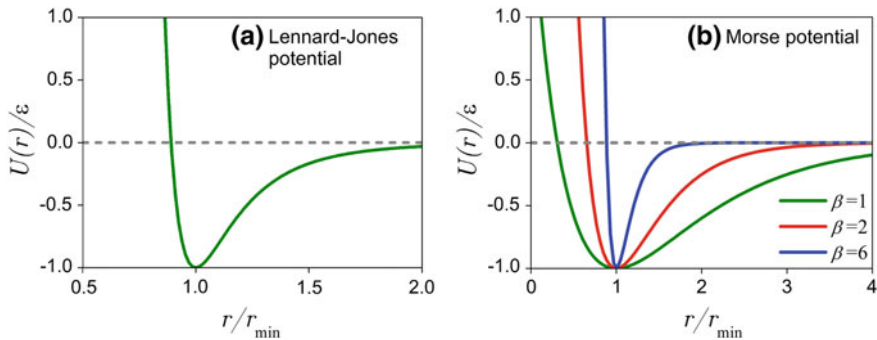


**Fig. 2.4** *panel a.* The Lennard-Jones potential (2.17) (scaled by  $\varepsilon$ ) as a function of the radial distance  $r$  measured in  $r_{\min}$ . *panel b.* The Morse potential (2.18) (scaled by  $\varepsilon$ ) as a function of the radial distance  $r$ . The curves correspond to  $\kappa = 2$ ,  $r_0 = 1$  (arb. units) and for three indicated values of  $\beta$  (in arb. units)

The parameters entering the right-hand side of (2.17) are the depth of the potential well,  $\varepsilon$ , and the radial distance to the minimum,  $r_{\min}$ . Figure 2.4a illustrates the behaviour of the Lennard-Jones potential.

The Lennard-Jones potential is a relatively good and universal approximation and due to its simplicity is often used to describe the properties of gases, and to model dispersion and overlap interactions in molecular systems. It is particularly accurate for noble gas atoms and is a good approximation at long and short distances for neutral atoms and molecules.

### 2.3.1.5 Morse Potential

The Morse potential, proposed in Ref. [106], is a convenient model for the potential energy of a diatomic molecule. It is a better approximation for treating the vibrational structure of the molecule than the harmonic oscillator, because it explicitly includes the effects of bond breaking. It also accounts for the anharmonicity of chemical bonds.

In MBN EXPLORER, the Morse potential is implemented in the most general form

$$U(r_{ij}) = \varepsilon \left[ \exp(-\kappa\beta(r_{ij} - r_0)) - \kappa \exp(-\beta(r_{ij} - r_0)) \right]. \quad (2.18)$$

The parameter  $r_0$  is the radial distance to the minimum of the potential,  $\varepsilon(\kappa - 1)$  is the depth of the potential well, the parameters  $\beta$  (in units of inverse length) and  $\kappa$  (dimensionless) define the steepness of the potential.

The curves in Fig. 2.4b show the Morse potential calculated for several values of  $\beta$ .

### 2.3.1.6 Girifalco Potential

The Girifalco potential [107], which describes the effective pairwise potential of the fullerene-fullerene interaction, has the following parametrization

$$U(r_{ij}) = \frac{\beta}{s_{ij}} \left[ \frac{1}{(s_{ij} - 1)^9} + \frac{1}{(s_{ij} + 1)^9} - \frac{2}{s_{ij}^9} \right] - \frac{\alpha}{s_{ij}} \left[ \frac{1}{(s_{ij} - 1)^3} + \frac{1}{(s_{ij} + 1)^3} - \frac{2}{s_{ij}^3} \right] \quad (2.19)$$

where  $s_{ij} = r_{ij}/2a$  and

$$\alpha = \frac{N^2 A}{12(2a)^6}, \quad \beta = \frac{N^2 B}{90(2a)^{12}}.$$

Here  $a$ ,  $A$  and  $B$  are the parameters of the potential and  $N$  is the number of atoms in the fullerene.

### 2.3.1.7 Dzugutov Potential

The Dzugutov pairwise potential is known to favor icosahedral ordering in the first neighbour shell and was originally developed as a model of simple glass-forming liquid metals [108]. The potential is constructed to suppress crystallization common to most monoatomic systems by the introduction of a repulsive term representing the Coulomb interactions that are present in a liquid metal. This term gives rise to a maximum that is needed to prevent particles residing in the second neighbour shell from finding energetically favorable sites as in an FCC or BCC configuration [109].

The Dzugutov potential reads as

$$U(r_{ij}) = A \left( \frac{1}{r_{ij}^m} - B \right) \exp \left( \frac{c}{r_{ij} - a} \right) \Theta(a - r_{ij}) + B \exp \left( \frac{d}{r_{ij} - b} \right) \Theta(b - r_{ij}), \quad (2.20)$$

where  $\Theta(x)$  is the Heaviside step function:

$$\Theta(x) = \begin{cases} 1, & \text{if } x > 0 \\ 0, & \text{if } x < 0 \end{cases}. \quad (2.21)$$

The parameters  $a$ ,  $b$ ,  $c$  and  $d$  are measured in units of length,  $m$  is an integer, the units of  $A$  and  $B$  are not fixed.

The curves in Fig. 2.5a illustrate the behaviour of the Dzugutov potential for several values of the parameter  $a$  (as indicated) and for fixed values of other parameters as they are specified in Ref. [108].

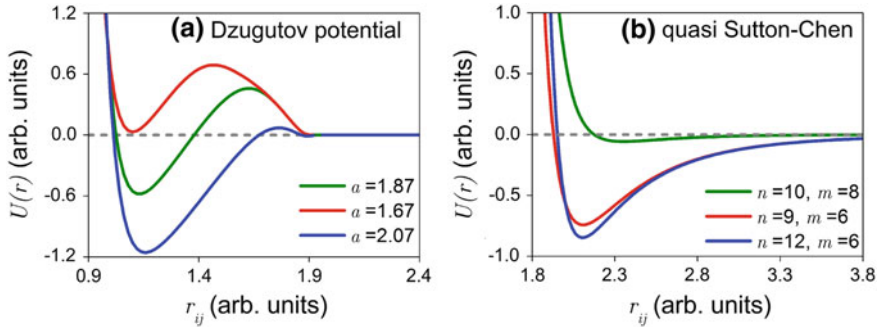


**Fig. 2.5** *panel a.* The Dzugutov potential (2.20) as a function of the radial distance  $r$ . The curves correspond to  $b = 1.94$ ,  $c = 1.1$ ,  $d = 0.27$ ,  $A = 5.82$ ,  $B = 1.28$  (all in arb. units),  $m = 16$ , and to three values of  $a$  (arb. units) as indicated. *panel b.* The Quasi Sutton-Chen potential (2.22) as a function of the radial distance  $r$ . The curves correspond to  $r_0 = 1$ ,  $a = 1$ ,  $b = 100$  (arb. units) and for three indicated sets of the integers  $n$  and  $m$

### 2.3.1.8 Quasi Sutton-Chen Potential

The pairwise Quasi Sutton-Chen potential is a pairwise potential, which is a simplified version of the many-body Sutton-Chen potential [54] discussed below in Sect. 2.3.2.1. The quasi Sutton-Chen potential is more convenient in some simulations because of its simple parametrisation, which has the following form:

$$U(r_{ij}) = \begin{cases} +\infty, & r_{ij} < r_0 \\ \frac{a}{(r_{ij} - r_0)^n} - \frac{b}{r_{ij}^m}, & r_{ij} \geq r_0 \end{cases}, \quad (2.22)$$

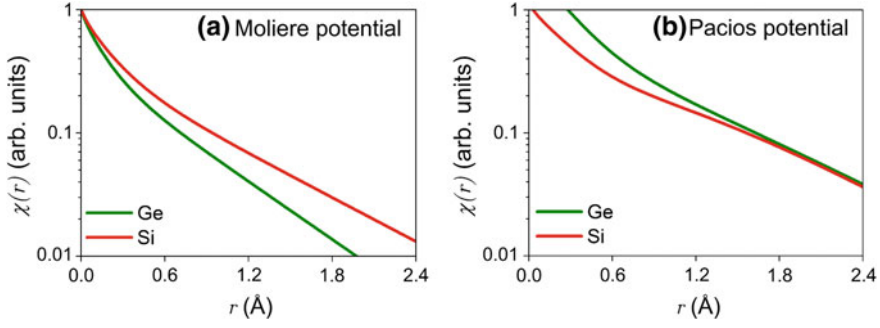
where  $n, m$  are integers, the parameter  $r_0$  is measured in units of length, and the parameters  $a, b$  are measured in  $[\text{Energy Length}^n]$  and  $[\text{Energy Length}^m]$ , respectively.

Figure 2.5b illustrates the quasi Sutton-Chen potential calculated for several sets  $(n, m)$  (as indicated) and for fixed values of other parameters as specified in the caption.

### 2.3.1.9 Yukawa Potential

The Yukawa potential [110] describes the pairwise interaction between two charges  $q_i$  and  $q_j$  one of which is fully screened (e.g., a nucleus of a neutral atom) as

$$U(r_{ij}) = A \frac{q_i q_j}{\varepsilon} \frac{e^{-\alpha r_{ij}}}{r_{ij}}. \quad (2.23)$$



**Fig. 2.6** Screening function  $\chi(r)$  calculated within the frameworks of the Moliere (*panel a*) and the Pacios (*panel b*) approximations, Eqs. (2.24) and (2.25). Two sets of the curves correspond to neutral silicon (red) and germanium (green) atoms

Here  $A$  and  $\varepsilon$  are dimensionless parameters, and the screening factor  $\alpha$  (measured in units of inverse length) defines the screening radius,  $1/\alpha$ .

### 2.3.1.10 Molière potential

The Molière potential [111] is another parametrisation which describes interaction between a net charge and a fully screened one. It can be written as a product of the Coulomb potential (2.16) and a function  $\chi(r_{ij})$  which accounts for the screening effect:

$$U(r_{ij}) = \frac{q_i q_j}{\varepsilon r_{ij}} \chi(r_{ij}), \quad \chi(r_{ij}) = \sum_{k=1}^3 \alpha_k e^{-\frac{\beta_k r_{ij}}{a_{TF}}}. \quad (2.24)$$

Here  $a_{TF}$  is the Thomas-Fermi radius of the atom,  $\alpha_k, \beta_k$  ( $k = 1, 2, 3$ ) are the dimensionless parameters of the potential. Their canonical values are:  $\alpha_{1,2,3} = (0.35; 0.55; 0.1)$  and  $\beta_{1,2,3} = (0.3; 1.2; 6.0)$ .

The curves in Fig. 2.6a represent  $\chi(r)$  calculated for neutral silicon and germanium atoms.

### 2.3.1.11 Pacios Potential

The Pacios potential [112] is the third potential implemented in MBN EXPLORER that describes the pairwise interaction between a charge and a screened atom. It has the same general form as that presented by Eq. (2.24) but differs in the definition of the screening function  $\chi$ :



$$\chi(r_{ij}) = 4\pi \sum_{k=1}^K \frac{\alpha_k}{\beta_k^3} (2 + \beta_k r_{ij}) e^{-\beta_k r_{ij}}. \quad (2.25)$$

The number  $N$  of the parameters  $\alpha_k$  and  $\beta_k$  as well as their values differ from atom to atom. Explicit values can be found in [112].

In the cited paper it is shown that the parametrisation (2.25) reproduces quite accurately the screened functions of various atoms calculated numerically within the framework of the Hartree-Fock approximation.

### 2.3.2 Many-Body Potentials

The total potential energy of the system consisting of  $N$  particles (atoms) which interact via a many-body potential is calculated as:

$$U_{\text{tot}} = \sum_{i=1}^N U_i(\{\mathbf{r}_i\}). \quad (2.26)$$

In the most general case, the energy term  $U_i(\{\mathbf{r}_i\})$ , which describes the interaction of the  $i$ th atom with other particles in the system, depends on the position of all atoms in the system. i.e.  $\{\mathbf{r}_i\} = \{\mathbf{r}_1, \mathbf{r}_2, \dots, \mathbf{r}_{i-1}, \mathbf{r}_{i+1}, \dots, \mathbf{r}_N\}$ . Below in this section we present the dependencies of the many-body interaction energy on atomic coordinates and discuss the choice of parameters of various potentials implemented in MBN EXPLORER.

#### 2.3.2.1 Sutton-Chen Potential

The Sutton-Chen potential is often employed for the description of the interaction between metal atoms, e.g., those which constitute a metallic cluster or a nanoparticle [54]. The total potential energy of  $N$  atoms can be written as a sum of the repulsive,  $U_R$ , and the attractive,  $U_A$ , terms:

$$U_{\text{tot}} = U_R + U_A, \quad (2.27)$$

The repulsive part of the Sutton-Chen potential is written in terms of the sum of pairwise power potentials (2.14):

$$U_R = \frac{\varepsilon}{2} \sum_{j \neq i}^N U(r_{ij}), \quad U(r_{ij}) = \left( \frac{a}{r_{ij}} \right)^n. \quad (2.28)$$

The attractive term accounts for the non-local effects of the interatomic interaction and is written as follows:

$$U_A = -c\varepsilon \sum_{i=1}^N \sqrt{\rho(r_i)}, \quad \rho(r_i) = \sum_{\substack{j=1 \\ j \neq i}}^N \left( \frac{a}{r_{ij}} \right)^m. \quad (2.29)$$

In these formulae, the parameters of the Sutton-Chen potential are introduced:  $\varepsilon$  (measured in units of energy),  $a$  and  $c$  (in units of length), and dimensionless integers  $n, m$ . The details on the discussion of the physical meaning of the parameters can be found in the original paper [54] as well as in the papers where the Sutton-Chen potential was extensively employed [113, 114].

### 2.3.2.2 Gupta Potential

The Gupta family of potentials can be used to model a variety of metals [115, 116]. Similar to the Sutton-Chen potential, the Gupta potential can be written in the form indicated in Eq. (2.27) but with the repulsive and attractive parts expressed in terms of the exponential potentials:

$$U_R = A \sum_{j \neq i}^N U(r_{ij}), \quad U(r_{ij}) = \exp \left[ -p \left( \frac{r_{ij}}{r_0} - 1 \right) \right], \quad (2.30)$$

$$U_A = -\xi \sum_{i=1}^N \sqrt{\rho(r_i)}, \quad \rho(r_i) = \sum_{\substack{j=1 \\ j \neq i}}^N \exp \left[ -2q \left( \frac{r_{ij}}{r_0} - 1 \right) \right], \quad (2.31)$$

where the parameters  $A$  and  $\xi$  are measured in units of energy,  $r_0$  – in units of length, and  $p, q$  are dimensionless. More detailed information on the parameters as well as on their derivation can be found in the original paper [117].

### 2.3.2.3 Finnis-Sinclair Potential

Finnis-Sinclair potential can be used to model heterogeneous systems [118].

For a binary system which contains particles of the types  $\alpha$  and  $\beta$ , one writes the general form of this potential as follows:

$$U_{\text{tot}} = U_{\text{R}} + U_{\text{A}}, \quad (2.32)$$

$$U_{\text{R}} = \sum_i \sum_{j \neq i} A_{\alpha\beta} \exp \left[ -p_{\alpha\beta} \left( \frac{r_{ij}}{d_{\alpha\beta}} - 1 \right) \right], \quad (2.33)$$

$$U_{\text{A}} = - \sqrt{\sum_{j \neq i} \xi_{\alpha\beta}^2 \exp \left[ -2q_{\alpha\beta} \left( \frac{r_{ij}}{d_{\alpha\beta}} - 1 \right) \right]}, \quad (2.34)$$

where  $A_{\alpha\beta}$ ,  $p_{\alpha\beta}$ ,  $d_{\alpha\beta}$ ,  $\xi_{\alpha\beta}$ ,  $q_{\alpha\beta}$  are parameters of the interaction of the particles of the indicated types [119].

### 2.3.2.4 Brenner Potential

Another many-body potential implemented in MBN EXPLORER is the bond-order Brenner potential, which was developed in particular for studying the covalent-bond carbon-based materials [120]. For every atom in the system, the Brenner potential depends on the position of the nearest neighbours of this atom. The total potential energy of the system interacting via the Brenner potential reads as:

$$U_{\text{tot}} = \frac{1}{2} \sum_i \sum_{i \neq j} f_{\text{cut}}(r_{ij}) [U_{\text{R}}(r_{ij}) - b_{ij} U_{\text{A}}(r_{ij})]. \quad (2.35)$$

Here  $f_{\text{cut}}(r_{ij})$  is the cut-off function which limits the interaction of an atom to its nearest neighbours. It is defined as follows:

$$f_{\text{cut}}(r_{ij}) = \begin{cases} 1, & r_{ij} \leq R_1 \\ \frac{1}{2} \left( 1 + \cos \frac{r_{ij} - R_1}{R_2 - R_1} \pi \right), & R_1 < r_{ij} \leq R_2, \\ 0, & r_{ij} > R_2 \end{cases} \quad (2.36)$$

with  $R_1$  and  $R_2$  being parameters, which determine the range of the potential.

The functions  $U_{\text{R}}(r_{ij})$  and  $U_{\text{A}}(r_{ij})$  in (2.35) are the repulsive and the attractive energy terms of the potential, respectively. They are parametrised as

$$U_{\text{R}}(r_{ij}) = \frac{D_{\text{e}}}{S-1} \exp \left[ -\sqrt{2S} \lambda (r_{ij} - R_0) \right] \quad (2.37)$$

$$U_{\text{A}}(r_{ij}) = \frac{D_{\text{e}} S}{S-1} \exp \left[ -\sqrt{2/S} \lambda (r_{ij} - R_0) \right]. \quad (2.38)$$

The factor  $b_{ij}$  in Eq. (2.35), which is called a bond-order term, reads as

$$b_{ij} = [1 + \zeta_{ij}]^{-\delta}, \quad \zeta_{ij} = \sum_{k \neq i, j} f_{\text{cut}}(r_{ik}) g(\theta_{ijk}). \quad (2.39)$$

The function  $g(\theta_{ijk})$ , which depends on the angle  $\theta_{ijk}$  between bonds formed by the pairs of atoms  $(i, j)$  and  $(i, k)$ , is defined as follows:

$$g(\theta_{ijk}) = a_0 \left[ 1 + \frac{c_0^2}{d_0^2} - \frac{c_0^2}{d_0^2 + (1 + \cos \theta_{ijk})^2} \right]. \quad (2.40)$$

To define the Brenner potential one has to specify several parameters which enter Eqs. (2.36)–(2.40). These include  $D_e$  measured in units of energy,  $R_0$ ,  $R_1$ ,  $R_2$  (measured in units of length),  $\lambda$  (inverse length units), and dimensionless quantities  $S$ ,  $\delta$ ,  $a_0$ ,  $c_0$ ,  $d_0$ . Discussion on the physical meaning of these parameters one finds in Ref. [120].

### 2.3.2.5 Tersoff Potential

The Tersoff many-body potential, being similar to the Brenner one, has a more complicated form. Initially, it was derived to study the structure and energetics of carbon-based materials [121–123]. The total potential energy of a system calculated using the Tersoff potential has the form

$$U_{\text{tot}} = \frac{1}{2} \sum_i \sum_{i \neq j} f_{\text{cut}}(r_{ij}) [a_{ij} U_R(r_{ij}) - b_{ij} U_A(r_{ij})]. \quad (2.41)$$

The cutoff function  $f_{\text{cut}}(r_{ij})$  is defined as in Eq. (2.36). The repulsive  $U_R$  and attractive  $U_A$  energy terms in Eq. (2.41) are given by

$$U_R(r_{ij}) = A \exp(-\lambda_1 r_{ij}) \quad (2.42)$$

$$U_A(r_{ij}) = B \exp(-\lambda_2 r_{ij}), \quad (2.43)$$

where  $A$ ,  $B$ ,  $\lambda_1$  and  $\lambda_2$  are parameters of the potential.

In contrast to the Brenner potential, the Tersoff potential has two bond-order terms  $a_{ij}$  and  $b_{ij}$  which are defined as

$$a_{ij} = [1 + \alpha^n \eta_{ij}^n]^{-\delta}, \quad b_{ij} = [1 + \beta^n \zeta_{ij}^n]^{-\delta}. \quad (2.44)$$

accompanied by

$$\eta_{ij} = \sum_{k \neq i, j} f_{\text{cut}}(r_{ik}) \exp[\lambda_3^3 (r_{ij} - r_{ik})^3], \quad (2.45)$$

$$\zeta_{ij} = \sum_{k \neq i, j} f_{\text{cut}}(r_{ik}) g(\theta_{ijk}) \exp[\lambda_3^3 (r_{ij} - r_{ik})^3]. \quad (2.46)$$

The function  $g(\theta_{ijk})$  depends on the angle  $\theta_{ijk}$  between bonds formed by pairs of atoms  $(i, j)$  and  $(i, k)$ . For the Tersoff potential it has the following form:

$$g(\theta_{ijk}) = 1 + \frac{c_0^2}{d_0^2} - \frac{c_0^2}{d_0^2 + (h + \cos \theta_{ijk})^2}. \quad (2.47)$$

The Tersoff potential is defined by specifying several parameters which enter the expressions written above:  $A$ ,  $B$  (in units of energy),  $R_{1,2}$  (in units of length),  $\lambda_{1,2,3}$  (inverse length units), and dimensionless quantities  $\alpha$ ,  $\beta$ ,  $n$ ,  $c_0$ ,  $d_0$ ,  $h$ . Discussion on the nature of these parameters can be found in the cited papers.

### 2.3.2.6 Stillinger-Weber Potential

Simulation of the structure of carbon-like structures (for example, single diamond, Si and Ge crystals as well as of the superlattice  $\text{Si}_{1-x}\text{Ge}_x$ ) by means of molecular dynamics can be performed by means of bond-ordered Tersoff and Brenner potentials, described above. Another potential, allowing this is the Stillinger-Weber [124–126].

The Stillinger-Weber potential is written as a combination of two-body and three-body interactions (see also [127–129]):

$$U_{\text{tot}} = \sum_{i < j} V_2(i, j) + \sum_{i < j < k} V_3(i, j, k). \quad (2.48)$$

Here the first term stands for the contribution of the two-body interactions:

$$V_2(i, j) = \begin{cases} \varepsilon_{ij} A \left[ B \left( \frac{\sigma_{ij}}{r_{ij}} \right)^p - \left( \frac{\sigma_{ij}}{r_{ij}} \right)^q \right] \exp \left( \frac{r_{ij}}{\sigma_{ij}} - a \right)^{-1}, & \text{if } \frac{r_{ij}}{\sigma_{ij}} < a \\ 0, & \text{if otherwise} \end{cases} \quad (2.49)$$

Dimensionless parameters  $A$ ,  $B$ , as well as the cut-off radius  $a$  are used to tune the pairwise potential. If the system in question consists of identical atoms, then for all pairs  $(i, j)$  the energy parameters  $\varepsilon_{ij}$  and the length ones  $\sigma_{ij}$  are set equal, i.e.  $\varepsilon_{ij} \rightarrow \varepsilon$ ,  $\sigma_{ij} \rightarrow \sigma$ . For a binary system, which consists of the atoms of two types, “1” and “2” (e.g., a Si-Ge superlattice) one introduces  $\varepsilon_{\alpha\beta} = \sqrt{\varepsilon_\alpha \varepsilon_\beta}$  and  $\sigma_{\alpha\beta} = (\sigma_\alpha + \sigma_\beta)/2$  ( $\alpha, \beta = 1, 2$ ).

The three-body interaction is parametrised as

$$\begin{aligned} V_3(i, j, k) = & \varepsilon_{ijk} h \left( \frac{r_{ij}}{\sigma_{ij}}, \frac{r_{ik}}{\sigma_{ik}}, \theta_{ijk} \right) \Theta \left( a - \frac{r_{ij}}{\sigma_{ij}} \right) \Theta \left( a - \frac{r_{ik}}{\sigma_{ik}} \right) \\ & + \varepsilon_{jik} h \left( \frac{r_{ji}}{\sigma_{ji}}, \frac{r_{jk}}{\sigma_{jk}}, \theta_{jik} \right) \Theta \left( a - \frac{r_{ji}}{\sigma_{ji}} \right) \Theta \left( a - \frac{r_{jk}}{\sigma_{jk}} \right) \\ & + \varepsilon_{kij} h \left( \frac{r_{ki}}{\sigma_{ki}}, \frac{r_{kj}}{\sigma_{kj}}, \theta_{kij} \right) \Theta \left( a - \frac{r_{ki}}{\sigma_{ki}} \right) \Theta \left( a - \frac{r_{kj}}{\sigma_{kj}} \right). \end{aligned} \quad (2.50)$$

Here,  $\Theta(x)$  is the Heaviside step function, Eq. (2.21),  $\theta_{ijk}$  is the angle between  $\mathbf{r}_{ij}$  and  $\mathbf{r}_{ik}$ , etc. The energy parameters  $\varepsilon_{ijk}$  are set equal in a homogenous material, but defines  $\varepsilon_{\alpha\beta\gamma} = \sqrt{\varepsilon_{\alpha\beta}\varepsilon_{\beta\gamma}}$  in the case of a binary structure  $((\alpha, \beta, \gamma) = 1, 2)$ . The function  $h$  is defined as

$$h\left(\frac{r_{ij}}{\sigma_{ij}}, \frac{r_{ik}}{\sigma_{ik}}, \theta_{ijk}\right) = \lambda_{ijk} \exp\left(\mu \left[ \left(\frac{r_{ij}}{\sigma_{ij}} - a\right)^{-1} + \left(\frac{r_{ik}}{\sigma_{ik}} - a\right)^{-1} \right]\right) \times \left(\cos \theta_{ijk} + \frac{1}{3}\right)^2 \quad (2.51)$$

where  $\lambda_{ijk}$  and  $\mu$  are dimensionless parameters.

## 2.4 Studying Biomolecules: The Force Field Concept and Beyond

### 2.4.1 Molecular Mechanics Force Field

Molecular mechanics (MM) potential is a special form of the potential energy of the system, widely used to describe the structure and properties of macromolecular systems, such as polypeptides, proteins and DNA [30, 32, 34, 130]. The form of the MM potential differs significantly from the pairwise and many-body potentials introduced in the earlier sections because it requires also the specification of the system topology (see Sects. 3.4 and 3.5).

The basic idea behind the MM potential is to account for all physically important interactions in a molecular system, i.e. the covalent interactions and the long range non-bonded interactions, using a simple parametric form of the potential. Thus, the total energy of the system interacting via the MM potential can be written as

$$U_{\text{tot}} = U_C + U_{\text{vdW}} + U_{\text{cov}}, \quad (2.52)$$

where  $U_C$  is the energy of the electrostatic (Coulomb) interaction, the term  $U_{\text{vdW}}$  stands for the energy of the van der Waals interactions, which are modeled in terms of the Lennard-Jones potential (see Sect. 2.3.1.4).

Below in this section we focus on the term  $U_{\text{cov}}$  which parametrises the energy associated with the covalent interactions. We stress that it is only applicable to the systems with a pre-defined topology since the latter defines the rules which determine the chemical bonds in the system. Thus, the energy of the covalent interactions is a sum over all such interactions. Real chemical bonds have a complex quantum mechanical nature. Therefore, the potential  $U_{\text{cov}}$  provides only a comparatively simple parametrisation describing the covalent interactions through a number of empirical parameters and fitting functions. The parameters of the potential are derived either from

experimental measurements of crystallographic structures, infrared spectra or on the basis of quantum mechanical calculations carried out for relatively small systems [31, 130, 131].

The term  $U_{\text{cov}}$  is constructed as follows:

$$U_{\text{cov}} = \sum_{\substack{\alpha=1 \\ i,j \in \alpha}}^{N_b} k_{ij}^{(b)} (r_{ij} - r_{ij,0})^2 + \sum_{\substack{\alpha=1 \\ i,j,k \in \alpha}}^{N_a} k_{ijk}^{(a)} (\theta_{ijk} - \theta_{ijk,0})^2 + \sum_{\substack{\alpha=1 \\ i,k \in \alpha}}^{N_{ub}} k_{ik}^{(ub)} (r_{ik}^{(ub)} - r_{ik,0}^{(ub)})^2 \\ + \sum_{\substack{\alpha=1 \\ i,j,k,l \in \alpha}}^{N_d} k_{ijkl}^{(d)} [1 + \cos(n_{ijkl} \chi_{ijkl} - \delta_{ijkl})] + \sum_{\substack{\alpha=1 \\ i,j,k,l \in \alpha}}^{N_{id}} k_{ijkl}^{(id)} (S_{ijkl} - S_{ijkl,0})^2. \quad (2.53)$$

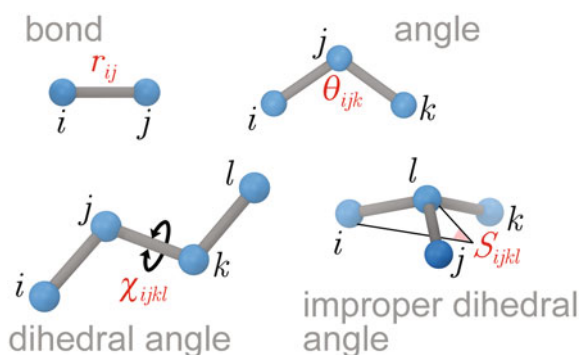
Here  $k_{ij}^{(b)}$ ,  $k_{ijk}^{(a)}$ ,  $k_{ik}^{(ub)}$ ,  $k_{ijkl}^{(d)}$ ,  $k_{ijkl}^{(id)}$ ,  $r_{ij,0}$ ,  $\theta_{ijk,0}$ ,  $r_{ik,0}^{(ub)}$ ,  $S_{ijkl,0}$ ,  $n_{ijkl}$ ,  $\delta_{ijkl}$  are the parameters of the potential. The collection of parameters for different molecular systems are often referred to as a force field [31, 130]. Different force fields were developed during the years and include for example the well established CHARMM [130] and AMBER [31]. The quantities  $r_{ij}$ ,  $\theta_{ijk}$ ,  $r_{ij}^{(ub)}$ ,  $\chi_{ijkl}$ ,  $S_{ijkl}$  are for independent variables (coordinates) which are illustrated by Fig. 2.7.

The first term on the right-hand side of Eq. (2.53) describes the potential energy arising due to stretching of the bonds between pairs of atoms in the system. Here,  $k_{ij}^{(b)}$  is the stiffness parameter,  $r_{ij,0}$  is the equilibrium distance and  $r_{ij}$  is the actual distance between atoms  $i$  and  $j$ , which form the bond with index  $\alpha$ . The summation is carried out over all topologically defined bonds of the, total number  $N_b$ .

The second term represents the potential energy arising due to the change of angles between every topologically defined triple of atoms in the system. Here,  $\theta_{ijk}$  stands for the angle between  $\mathbf{r}_{ij}$  and  $\mathbf{r}_{jk}$  (see Fig. 2.7),  $\theta_{ijk,0}$  is the equilibrium value of this angle and  $k_{ijk}^{(a)}$  is the stiffness parameter. The summation is performed over different triples of the total number  $N_a$ .

The third term, commonly referred to as the Urey-Bradley term, is also related to the “angular” interactions in the system. It corresponds to a fictional interaction

**Fig. 2.7** Internal coordinates for molecular mechanics interactions:  $r_{ij}$  governs bond stretching;  $\theta_{ijk}$  represents the angle term;  $\chi_{ijkl}$  gives the dihedral angle; the small out-of-plane angle  $S_{ijkl}$  is governed by the so-called “improper” dihedral angle



between the first,  $i$ , and the third,  $k$ , atoms in every topologically defined triple of atoms in harmonic approximation. The  $k_{ik}^{(\text{ub})}$  is the stiffness parameter for this interaction,  $r_{ik,0}^{(\text{ub})}$  is the equilibrium distance between the atoms, and  $N_{\text{ub}}$  is the total number of such interactions.

The fourth term in Eq.(2.53) describes the torsion energy. It is characterised through a dihedral angle  $\chi_{ijkl}$  formed by four atoms,  $i$ ,  $j$ ,  $k$  and  $l$ , connected via chemical bonds (see Fig. 2.7). The “multiplicity”  $n_{ijkl}$  is typically set to 1, 2, or 3,  $k_{ijkl}^{(\text{d})}$  is the dihedral spring constant.

The last term in Eq. (2.53) describes the so-called improper dihedral angles, which are used in the molecular topology to maintain planarity. As such, the harmonic form with a large spring constant  $k_{ijkl}^{(\text{id})}$  and equilibrium value  $S_{ijkl,0}$  (typically equal to zero) is used to restrain configuration of an atom and three atoms bonded to it. Similar to the case of dihedral angles,  $S_{ijkl}$  is the angle between the plane containing the first three atoms with indices  $(ijk)$  and the plane containing the last three atoms with the indices  $(jkl)$  which define this dihedral angle.

For further referencing let us present explicit formulae for the forces which appear due to the MM potential  $U_{\text{cov}}$ . In this case, it is more convenient to calculate separately the partial forces acting on each atom due to the “bond”, “angle”, Urey-Bradley, “dihedral” and “improper dihedral” interactions rather than to evaluate the total force as it is done for pairwise and many-body interactions. Details of the evaluation can be found in [59].

The forces  $\mathbf{F}_{i,j}^{(\text{b})}$  acting on the atoms  $i$  and  $j$  bound by the bond interaction read:

$$\mathbf{F}_i^{(\text{b})} = -\mathbf{F}_j^{(\text{b})} = 2k_{ij}^{(\text{b})}(r_{ij} - r_{ij,0}) \mathbf{n}_{ij} \quad (2.54)$$

where  $\mathbf{n}_{ij} = \mathbf{r}_{ij}/r_{ij}$ .

The forces  $\mathbf{F}_{i,j,k}^{(\text{a})}$  in a triple system of atoms with indices  $i$ ,  $j$  and  $k$  bound by the angular interaction are calculated as follows:

$$\begin{cases} \mathbf{F}_i^{(\text{a})} = -2k_{ijk}^{(\text{a})} \frac{\theta_{ijk} - \theta_{ijk,0}}{\sin \theta_{ijk}} \frac{\mathbf{n}_{jk} - \mathbf{n}_{ij} \cos \theta_{ijk}}{r_{ij}} \\ \mathbf{F}_k^{(\text{a})} = -2k_{ijk}^{(\text{a})} \frac{\theta_{ijk} - \theta_{ijk,0}}{\sin \theta_{ijk}} \frac{\mathbf{n}_{ij} - \mathbf{n}_{jk} \cos \theta_{ijk}}{r_{jk}} \\ \mathbf{F}_j^{(\text{a})} = -(\mathbf{F}_i^{(\text{a})} + \mathbf{F}_k^{(\text{a})}) \end{cases} \quad (2.55)$$

In the same system, the Urey-Bradley interaction gives rise to the following forces:

$$\mathbf{F}_i^{(\text{ub})} = -\mathbf{F}_k^{(\text{ub})} = 2k_{ik}^{(\text{ub})}(r_{ik} - r_{ik,0}^{(\text{ub})}) \mathbf{n}_{ik} . \quad (2.56)$$

The “dihedral” interaction appears due to the change of the dihedral angle  $\chi \equiv \chi_{ijkl}$  (see Fig. 2.7) in a system of four topologically defined particles  $i$ ,  $j$ ,  $k$  and  $l$ . Here,  $\chi$  is defined as the angle between the plane containing the  $i$ ,  $j$  and  $k$  atoms and



that containing the atoms  $j, k$  and  $l$ . The forces  $\mathbf{F}_v^{(d)}$  acting on the atoms  $v = i, j, k, l$  are given by

$$\begin{cases} \mathbf{F}_i^{(d)} = \kappa \mathbf{D}_A \times \mathbf{r}_{jk} \\ \mathbf{F}_j^{(d)} = -\kappa (\mathbf{D}_A \times \mathbf{r}_{jk} + \mathbf{D}_B \times \mathbf{r}_{jk}) \\ \mathbf{F}_k^{(d)} = -\kappa (\mathbf{D}_A \times \mathbf{r}_{ij} - \mathbf{D}_B \times \mathbf{r}_{jk} - \mathbf{D}_B \times \mathbf{r}_{kl}) \\ \mathbf{F}_l^{(d)} = \kappa (\mathbf{D}_A \times \mathbf{r}_{ij} - \mathbf{D}_B \times \mathbf{r}_{kl}) \end{cases} \quad (2.57)$$

where the following notations are used:

$$\kappa = -k_{ijkl}^{(d)} n_{ijkl} \frac{\sin(n_{ijkl}\chi - \delta_{ijkl})}{\sin \chi}, \quad (2.58)$$

$$\mathbf{D}_A = \frac{\mathbf{B} - \mathbf{A} \cos \chi}{|\mathbf{A}|}, \quad \mathbf{D}_B = \frac{\mathbf{A} - \mathbf{B} \cos \chi}{|\mathbf{B}|}, \quad (2.59)$$

$$\mathbf{A} = \mathbf{r}_{ij} \times \mathbf{r}_{jk}, \quad \mathbf{B} = \mathbf{r}_{jk} \times \mathbf{r}_{kl}. \quad (2.60)$$

Finally, the potential due to the improper dihedral angle interaction results in the forces  $\mathbf{F}_v^{(id)}$  acting on the atoms  $v = i, j, k, l$  in a system of four topologically defined particles:

$$\begin{cases} \mathbf{F}_i^{(id)} = 2k_{ijkl}^{(id)} (S_{ijkl} - S_{ijkl,0}) (\mathbf{D}_A \times \mathbf{r}_{jk}) \\ \mathbf{F}_j^{(id)} = -2k_{ijkl}^{(id)} (S_{ijkl} - S_{ijkl,0}) (\mathbf{D}_A \times \mathbf{r}_{jk} + \mathbf{D}_B \times \mathbf{r}_{jk}) \\ \mathbf{F}_k^{(id)} = -2k_{ijkl}^{(id)} (S_{ijkl} - S_{ijkl,0}) (\mathbf{D}_A \times \mathbf{r}_{ij} - \mathbf{D}_B \times \mathbf{r}_{jk} - \mathbf{D}_B \times \mathbf{r}_{kl}) \\ \mathbf{F}_l^{(id)} = 2k_{ijkl}^{(id)} (S_{ijkl} - S_{ijkl,0}) (\mathbf{D}_A \times \mathbf{r}_{ij} - \mathbf{D}_B \times \mathbf{r}_{kl}) \end{cases} \quad (2.61)$$

To model molecular interactions in a wider range of biological processes, the standard molecular mechanics potentials should be improved. The CHARMM force field employs harmonic approximation for describing the interatomic interactions, thereby limiting its applicability to small deformations of the molecular system. In case of larger perturbations the potential should decrease to zero as the valence bonds rupture. The rupture of valence bonds causes the involved angular and dihedral interactions to vanish as well. MBN EXPLORER permits simulations with the rupture of covalent bonds by using a dissociative CHARMM potential [61] as described below.

### 2.4.2 Rupture of Covalent Bonds

To model rupture of covalent bonds, MBN EXPLORER uses modified potentials which describes the interactions of atoms connected by chemical bonds. The standard CHARMM force field treats the covalent interactions of two atoms within the harmonic approximation,  $U_{ij}^{(b)} = k_{ij}^{(b)} (r_{ij} - r_{ij,0})^2$  (see the first term on the right-hand side of Eq. (2.53)). This parametrisation describes well the bond stretching in

the case of small displacements  $r_{ij} - r_{ij,0}$  but gives erroneous results as the displacement increases. For a satisfactory quantitative description of the covalent bond rupture, it is reasonable to use the Morse potential approximation instead of the harmonic one. The Morse potential requires an additional parameter which accounts for the energy of the bond dissociation. For a pair of atoms, the Morse potential reads:

$$U_M(r_{ij}) = D_{ij} \left( e^{-2\beta_{ij}(r_{ij}-r_{ij,0})} - 2e^{-\beta_{ij}(r_{ij}-r_{ij,0})} \right), \quad (2.62)$$

where  $D_{ij}$  is the dissociation energy of the bond and parameter  $\beta_{ij}$  determines the steepness of the potential.

For small displacements the right-hand side of (2.62) is approximated by the quadratic form

$$U_M(r_{ij}) \approx -D_{ij} + \beta_{ij}^2 D_{ij} (r_{ij} - r_{ij,0})^2, \quad (2.63)$$

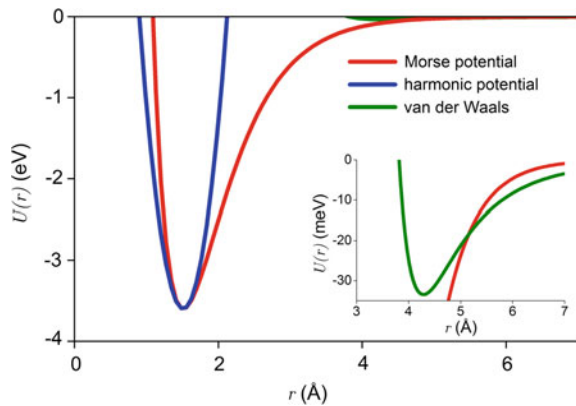
which allows one to relate  $D_{ij}$  and  $\beta_{ij}$  to the stiffness parameter  $k_{ij}^{(b)}$  employed in the harmonic approximation:

$$\beta_{ij} = \sqrt{k_{ij}^{(b)} / D_{ij}}. \quad (2.64)$$

Figure 2.8 illustrates the Morse potential which models the interaction of two carbon atoms of the CN7-CN8B type according to the CHARMM nomenclature [130]. This covalent bond arises, for example, between the C4'-C5' atoms of ribose. At small displacements from the equilibrium distance  $r_{ij,0}$ , the Morse and the harmonic potentials are close to each other. As the interatomic distance increases, the atoms start to interact through polarization forces, modeled in terms of the Lennard-Jones potential. The comparison between the Morse and Lennard-Jones potentials at larger distances is shown in the inset.

Note that the parametrisation of the bonded interactions introduced in Eq. (2.63) is only applicable for studying bond dissociation. It has been implemented in MBN

**Fig. 2.8** The pairwise carbon-carbon (CHARMM type CN7-CN8B) interaction potential in the harmonic and the Morse approximations. The van der Waals interaction is illustrated by the *green* curve in the inset. Adapted from [61]



EXPLORER as it essentially relies on the classical CHARMM force field, and requires a minimal number of extra parameters (only dissociation energy of a bond is needed) to study covalent bond dissociation. However, this approach is hardly applicable to study bond formation, as one would require to provide the program with all possible combinations of chemical bonds in a molecular system. Additionally, charge redistribution should be considered carefully upon chemical bond formation. The charge redistribution effect is neglected in the present parametrisation, therefore, limiting its applicability to the situations when only a few chemical bonds are expected to be broken.

### 2.4.3 Rupture of Valence Angles

The rupture of chemical bonds in the course of a simulation automatically employs an improved potential for the valence angles. The CHARMM force field uses the harmonic approximation to parametrise the potential associated with the change of a valence angle between bonds with indices  $ij$  and  $jk$  reads as:  $U_{ijk}^{(a)} = k_{ijk}^{(a)} (\theta_{ijk} - \theta_{ijk,0})^2$  (see the second term on the right-hand side of (2.53)). This potential grows unrestrictedly leading to potentially nonphysical results for large values of  $|\theta_{ijk} - \theta_{ijk,0}|$ . To avoid this, the harmonic potential can be substituted with

$$U_{ijk}^{(\cos)} = 2k_{ijk}^{(a)} [1 - \cos(\theta_{ijk} - \theta_{ijk,0})]. \quad (2.65)$$

This parametrisation, while reducing to the harmonic approximation at small variations of the angle, provides the energy threshold that becomes important when studying rupture of covalent bonds occurring at larger angles.

The rupture of a covalent bond is accompanied by a rupture of the associated angular interactions. The effect of bond rupture on the angular potential can be modeled by means of the function  $\sigma(r_{ij})$  defined as follows:

$$\sigma(r_{ij}) = \frac{1}{2} [1 - \tanh \beta_{ij} (r_{ij} - r_{ij,b})], \quad (2.66)$$

where  $r_{ij,b} = (R_{ij}^{\text{vdW}} + r_{ij,0})/2$ . This function introduces a correction (in the form of a smoothed step function) of the angular interaction potential, assuming the distance between a pair of atoms involved in the angular interaction increases from the equilibrium value,  $r_{ij,0}$ , to the van der Waals contact value  $R_{ij}^{\text{vdW}}$ . Figure 2.9 illustrates the behaviour of  $\sigma(r)$ .

Since an angular interaction depends on two bonds associated with the atom indices  $ij$  and  $ik$ , the potential energy,  $\tilde{U}_{ijk}^{(a)}$ , describing the valence angular interaction that is subject to rupture is parameterized as follows [61]:

$$\tilde{U}_{ijk}^{(a)} = \sigma(r_{ij})\sigma(r_{jk})U_{ijk}^{(\cos)}. \quad (2.67)$$

**Fig. 2.9** The switching function (2.66) calculated for the carbon-carbon (CHARMM type CA-CA) interaction

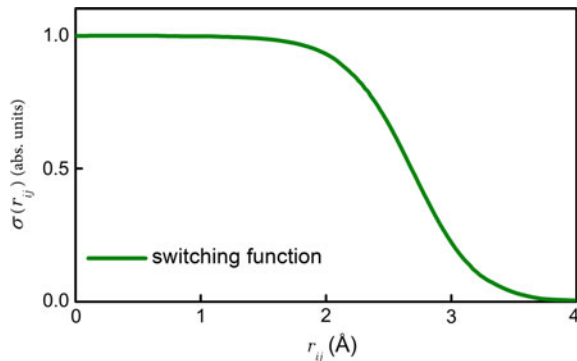
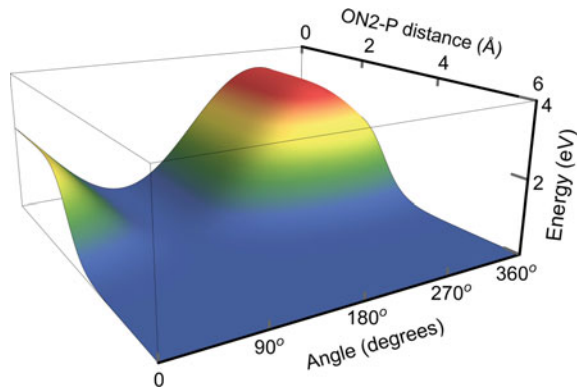


**Fig. 2.10** The CN8B-ON2-P angular potential calculated using Eq. (2.67) with account for the ON2-P bond rupture. Adapted from [61]



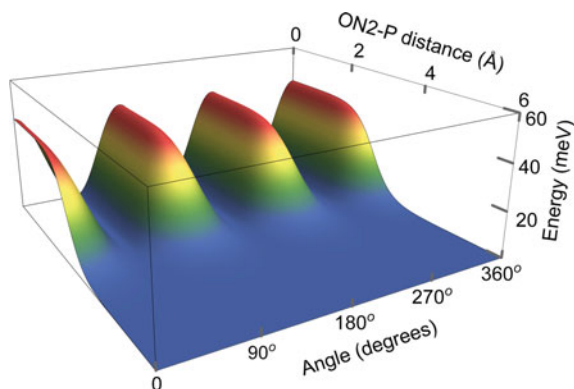
The angular potential decreases as either the bond length between atoms  $ij$  or  $jk$  increases. Figure 2.10 illustrates the behaviour of  $\tilde{U}_{ijk}^{(a)}$  for the system CN8B-ON2-P, which arises, for instance, when modelling DNA nucleotides. The plot corresponds to the rupture of the bond between the oxygen and the phosphorous while the CN8B-ON2 bond length is taken equal to its equilibrium value,  $r_{ij,0}$ .

The forces acting on atoms  $i$ ,  $j$  and  $k$  bound through potential  $\tilde{U}_{ijk}^{(a)}$  are evaluated similarly to the forces in the regular angular interactions of the CHARMM force field (see Eq. (2.55)). The corresponding formulae one finds in [59].

### 2.4.4 Rupture of Dihedral Interactions

As mentioned, in conventional MM the “dihedral” interactions arise due to the change of the dihedral angles between every four topologically defined atoms, see Fig. 2.7. For a group of four atoms  $i$ ,  $j$ ,  $k$  and  $l$ , the potential  $U_{ijkl}^{(d)}$  depends on the angle  $\chi_{ijkl}$  between the planes containing atoms  $(ijk)$  and  $(jkl)$ . In the harmonic approximation this potential reads

**Fig. 2.11** The CN4-P-ON2-CN7 dihedral potential calculated using Eq. (2.69) with account for the ON2-P bond rupture. Adapted from [61]



$$U_{ijkl}^{(d)} = k_{ijkl}^{(d)} (1 + \cos(n_{ijkl} \chi_{ijkl} - \delta_{ijkl})) , \quad (2.68)$$

(see the forth term on the right-hand side of (2.53)).

The dihedral interactions also become disturbed upon the covalent bond rupture and, therefore, Eq. (2.68) should be modified to take into account this effect. Since each dihedral interaction consists of a quadruple of atoms with indices  $i$ ,  $j$ ,  $k$  and  $l$ , the rupture of a dihedral interaction should take into account three bonds that contribute to this interaction. Thus, the modified potential energy with account for bond rupture is written as follows [61]

$$\tilde{U}_{ijkl}^{(d)} = \sigma(r_{ij})\sigma(r_{jk})\sigma(r_{kl})U_{ijkl}^{(d)}, \quad (2.69)$$

where the  $\sigma$ -functions are defined in Eq. (2.66).

Figure 2.11 shows a typical profile of the dihedral potential with account for bond rupture. In this case we have considered the CN4-P-ON2-CN7 dihedral interaction, where the middle ON2-P bond was broken. This interaction is important when modelling bond breaks in DNA nucleotides.

### 2.4.5 Formation of New Bonds

Rupture of covalent bonds leads to formation of individual atoms, radicals or smaller molecules. In order to properly simulate the chemical balance in the system one has to allow for new bonds to be formed within the system.

In MBN EXPLORER, after the rupture of a chemical bond between a pair of atoms, these atoms are placed in a special list of chemically active atoms. Only the atoms from this list can participate in chemical reactions and form new bonds. For each of atoms of the list the number of possible molecular bonds is stored, and is determined by the atom's valence.

In order to create new bonds in the system the list of chemically active atoms is evaluated at each simulation step and the neighbouring atoms are selected. A chemical bond is formed between a pair of atoms provided the following conditions are met: (i) the parameters of the bond for this combination of atoms are defined in the simulation input; (ii) atoms are modeled as bound through the Morse potential; and (iii) the distance between the atoms is less than the predefined cutoff/capture radius. If these three conditions are met simultaneously in the simulation the bond is created and the system's topology is updated. For each new covalent bond the neighbouring atoms are analyzed. If the parameters of angular bond are defined for some group of atoms such bond should be also formed.

#### **2.4.6 *Partial Charges Redistribution***

The rupture and formation of bonds leads to reconfiguration of the molecular systems and to redistribution of partial charges of atoms. The modification of MBN EXPLORER presented here accounts for this redistribution. The charge redistribution should obey the following conditions: the total charge of the systems is conserved, the total charge of each individual molecule is an integer in atomic system of units, i.e. an integer number of the electron charge. MBN EXPLORER supports the two options for modelling the charge redistribution process: (i) a general (default) one applicable to any molecules, and (ii) a special one redistributing charges within molecules according to the known electronic configurations.

The default mechanism of charge redistribution is activated upon rupture or formation of covalent bonds. In the case of a bond rupture, two newly emerged fragments of a molecular system have likely non-compensated, non-integer charges. The total charge of each of the newly emerged fragment is thus rounded to the closest integer value and the charge difference is transferred from one fragment to another. This difference is redistributed evenly among all atoms of the fragments. Upon the formation of new a bond, the charge is redistributed inside the newly created molecule in order to lower the values of partial charges preserving the initial sum of charges.

### **2.5 Multiscale Methods**

Atomistic processes that govern macroscopic phenomena in materials often have large activation barriers and, therefore, occur at time scales that are beyond the reach of conventional atomistic MD simulation techniques. Although recent developments of MD-based accelerated dynamics [132–134] have successfully extended the simulation time scales to microseconds, it still remains computationally inefficient to employ atomistic MD for a large class of important problems such as, e.g., diffusion, nucleation, growth, crystallization, defect evolution and chemical reactions. Kinetic Monte Carlo (KMC) method is often the tool of choice for studying dynamic

of processes occurring on long time scales, e.g., milliseconds to hours [9, 86, 87, 135–139]. Instead of propagating individual atoms in time, as done in MD, the KMC method models the evolution of a molecular coarse-grained system in a probabilistic way.

Available KMC-based methods allow to simulate processes of epitaxial thin film growth [136, 140], crystal growth [141], defect diffusion in metals and semiconductors [142], nanoparticle diffusion, and were employed for a number of biophysical applications [143, 144]. These existing methods deliver good agreement with experimental observations, but it should be noted that depending on the studied problem the algorithmic realization of the KMC approaches is usually different [136]. Our goal is to combine various approaches into a generalized KMC-based computer package that could naturally be customized for different systems and processes mentioned above.

Another type of case studies requiring multiscale descriptions involve irradiation driven transformation of molecular systems. In this case irradiation induced fast, local and random quantum processes embedded into a large scale molecular environment result in significant alterations of the entire system on the time scales much larger than the duration of irradiation. This kind of case studies can be tackled by means of the irradiation driven molecular dynamics (IDMD) introduced recently in [16], and discussed below in this section along with other multiscale methods mentioned above.

### 2.5.1 *Kinetic Monte Carlo Method*

The KMC approach could be used to study various bio-nano systems and processes, for example, nanopatterning in nanoengineering [145], nanomarkers dynamics in medical diagnostics [146], reactivity of nanoparticles with biological tissue, protein interactions in biology [147], cell budding [148], etc. In these examples the KMC approach appears to be useful, as all of the aforementioned systems consist of building blocks whose internal motion appears to be irrelevant for the macroscopic evolution of the entire system. In the most general case these building blocks could be treated as particles that move according to specific physical laws, determined by the particles' internal properties and the environment. The KMC approach described here deals with such coarse-grained particles and renders their dynamics in a probabilistic fashion. Below we discuss the underlying physical principles of the KMC approach and provide details of its implementation in MBN EXPLORER.

The classical KMC approach describes the time evolution of a system through a number of predefined kinetic process rates [135, 138]. In the most general case, it includes few steps, depicted in Fig. 2.12a [7]. The algorithm starts at a time instance  $t = 0$  (step 1) where the simulated system of interest is initialized. Next, the systems evolution is simulated iteratively (steps 2.1 and 2.2), while the simulation time increases by  $\Delta t$  (step 3) until it reaches the threshold value  $t^{(\text{final})}$  (step 4). Steps 2.1 and 2.2 form the computational core of the KMC algorithm, the so-called main

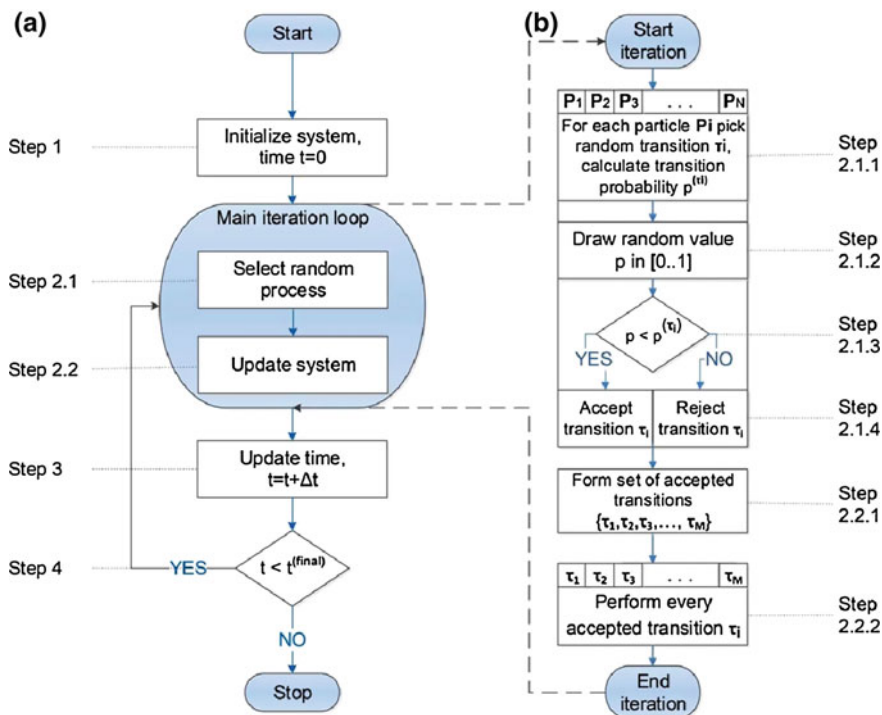


**Fig. 2.12** **a** Flow chart of the classical kinetic Monte Carlo algorithm [135, 138]. **b** The computational core of the suggested algorithm is provided through the main iteration loop. The figure is adapted from [7]

iteration loop. During this main iteration loop the KMC algorithm randomly selects one process from the pool of all possible stochastic processes in the system (step 2.1) and updates the system accordingly (step 2.2). The main iteration loop could be found in different realizations depending on the simulated system scale (atomic-size [149], molecule-size or higher scale [150]), modern efficiency requirements (serial [135] or parallel [137] implementation), or type of processes (diffusion [138], chemical reactions [135]). In Ref. [7] the state-of-the-art techniques were grouped to build a uniform, yet efficient algorithm which can potentially simulate a wide range of diffusion-driven physical processes in the three-dimensional space.

The main iteration loop of the suggested KMC algorithm updates the system as illustrated in Fig. 2.12b. Each stochastic process in the system is described through transitions of individual particles. The main iteration loop is, therefore, subdivided into two phases that include defining possible transitions for all particles in the system (steps 2.1.1–2.1.4) and performing transitions (steps 2.2.1 and 2.2.2). During the first phase each particle in the system is assigned a displacement direction vector, which is chosen randomly assuming that particles move isotropically in space. The displacement vector is then used to define the stochastic process  $\tau_i$  and the



corresponding probability  $p^{(\tau_i)}$  that such process occurs in the time span of a simulation step (step 2.1.1). Next (steps 2.1.2 and 2.1.3), the algorithm tests which transitions should be accepted or rejected, by validating the probability against a randomly generated number  $p^{(\tau_i)} \in [0..1]$ . The second phase of the main iteration loop collects all accepted transitions (step 2.2.1) and translates the particles accordingly (step 2.2.2), taking account for particle collisions, i.e., situations when particles attempt to occupy same sites.

### 2.5.2 *Simplifications of the KMC Method*

As it follows from the algorithm description above, one of the major computational advantages of the KMC method, compared to atomistic MD, arises due to an increase of the simulation time step used in the KMC approach. This advantage arises due to the course-graining of a molecular system and the model assumptions made.

Another simplification of the KMC method, leading to significant acceleration of the calculations, is achieved through introducing a virtual lattice, as also done previously [136, 138], into the simulations that hosts the particles of the system in a regular fashion. The topology of this lattice creates a trade-off between positioning precision and the computational efficiency. In the three-dimensional space one can use different lattice types, based on hcp, fcc close-packing, rhombic dodecahedron and cubic tessellations. For the best simulation efficiency we have chosen the cubic lattice; in this case the simulation space is tessellated with virtual cubic cells. Every particle in the system is allowed to occupy one cell. By introducing particles into the lattice we assume the geometry and orientation of the particles as fixed. In other words, when a particle is displaced in a certain direction, all its constituent parts are translated accordingly. Several particles cannot share the same cell, therefore, once two particles get in contact, they interact.

Introducing a lattice into simulation allows one to accelerate computations significantly. In this case it becomes possible to update coordinates of particles only upon their transition to neighbouring cells, which occur significantly less frequent than in MD, where the state of each particle should be updated on every simulation step. The transition of particles in the kinetic approach is calculated through the transition rates (discussed below) and is computationally cheaper than the force evaluation in conventional MD. Indeed, the number of operations needed to obtain transition probability for a particle in the KMC approach is  $O(N_n)$ , where  $N_n$  is the number of cells neighbouring to a given particle. The linked cell algorithm [151] (see also Sect. 2.6.2 below), often used in MD, employs similar approach, and has the computational cost  $O(N_n N_c)$ , where  $N_c$  stands for the average number of particles in a cell. However, a strong inequality  $N_c \gg 1$  makes the linked cell algorithm more computationally demanding than the KMC approach.

### 2.5.3 Particle Dynamics Model

The dynamics of particles in the system is driven by inter-particle interactions. In the discussed model the interaction between distant particles is neglected, limiting it by the nearest neighbours. Such approach is justified for systems without long-range forces, i.e., where the short-range interaction is prevailing.

An isolated particle has an equal probability to move in all directions in the three-dimensional space. Thus, by introducing a simulation lattice, a particle in the system could experience different motions (26 possible motion directions for a particle on a cubic lattice) from one cell to another during a time interval  $\Delta t$ , which we denote as the simulation time step. Each possible movement of a particle during  $\Delta t$  is further denoted as particle transition. The step  $\Delta t$  should be chosen such that a particle experiencing the fastest motion relocates itself to the neighbouring cell during the time step. Formally, this means that any particle in the system in average could not diffuse further than the cell size  $d_0$  over the interval  $\Delta t$ . The transition vector of a particle is chosen randomly with respect to the isotropic motion and then mapped to one of the 26 possible directions of the cubic lattice. The probability  $p^{(\tau)}$  that a particle will undergo a certain transition  $\tau$  during the time step  $\Delta t$  reads as

$$p^{(\tau)} = \Gamma^{(\tau)} \Delta t, \quad (2.70)$$

where  $\Gamma^{(\tau)}$  is the rate of this transition. In the following text, we omit the superscript  $(\tau)$  for the sake of clarity. Assuming the Boltzmann type of dependence of rate on temperature, the rate  $\Gamma$  can be parametrised as

$$\Gamma = \Gamma_0 \exp(-E_a/k_B T). \quad (2.71)$$

Here  $E_a$  is the activation energy of the process  $\tau$ ,  $\Gamma_0$  is the pre-exponential factor,  $T$  is the temperature and  $k_B$  is the Boltzmann constant.

In a system of particles (atoms, molecules, nanoparticles, etc.) interacting through the short-range forces, the activation energy  $E_a$  can be expressed as a sum of the two major contributions  $E_b$  and  $E_{pd}$  accounting for the interparticle binding and the particle peripheral diffusion correspondingly:

$$E_a = E_b + E_{pd}. \quad (2.72)$$

The binding energy  $E_b$  describes the dissociation energy of two neighbouring particles, while the peripheral diffusion energy barrier  $E_{pd}$  is the energy necessary to displace a particle to a neighbouring cell without breaking its contact with other particles. In this respect, it is important to mention that particles separated by more than one cell are considered as noninteracting.

When a particle undergoes a transition, it typically overcomes an energy barrier separating its states before and after the transition. The barrier depends on the number and type of neighbouring particles before and after the transition. For each particle,

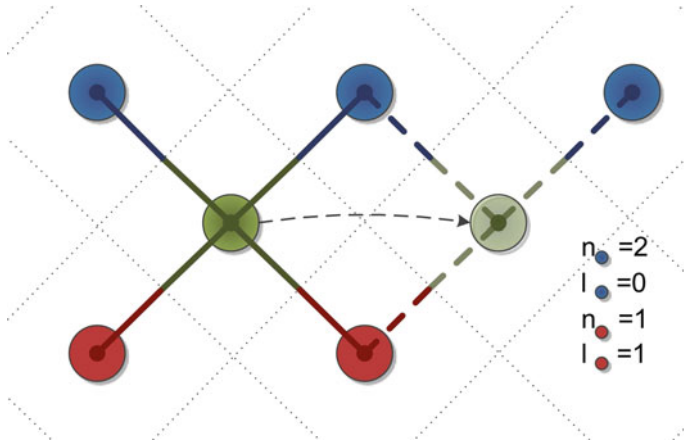


**Fig. 2.13** Top view on a *cubic* lattice (*dotted lines*) populated with particles (*circles*). A particle (*green*) surrounded by four particles of two different types (*blue* and *red*) is displaced right, i.e., to its vacant neighbouring site. In the course of this transition the number of the *red* type neighbours decreases by unity, i.e.,  $l(\text{red}) = 1$ , while the number of the *blue* type neighbours stays unchanged, i.e.,  $l(\text{blue}) = 0$ . The number of maintained neighbours  $n$  is equal to 2 for particles of the *blue* type and is equal to 1 in the case of *red* type particles. The figure is adapted from [7]

the number of neighbours is an intuitive measure used to characterise the effective interaction energy of a particle with the rest of the system. In this respect we consider different types of particles and count the number of neighbours of a given type for each particle separately. Let  $\mathcal{B}$  denote a set of all possible particle types in the system. In our model, we assume that the activation energy barrier  $E_a$  for a particle transition depends on the numbers of unneighboured particles  $\{l_j, j \in \mathcal{B}\}$  and the numbers of maintained neighbours  $\{n_j, j \in \mathcal{B}\}$  of each particle type. Let  $m_{\text{before}}(j)$  and  $m_{\text{after}}(j)$  denote the number of neighbours of a certain particle, being of type  $j$  before and after transition  $\tau$ , respectively. Then, the number of maintained and unneighboured particles could be defined as

$$n_j = \min\{m_{\text{before}}(j); m_{\text{after}}(j)\}, \quad l_j = \max\{m_{\text{before}}(j) - m_{\text{after}}(j); 0\}. \quad (2.73)$$

This particular definition of  $l_j$  and  $n_j$  is useful, as it allows one to avoid dependence of particle transition probability on a particular lattice type. Figure 2.13 illustrates schematically a transition of a particle and introduces the numbers  $l_j$  and  $n_j$  arising during this transition.

Knowing the sets of unneighboured and maintained neighbours at every instance of a simulation for each particle, allows one to establish the peripheral diffusion energy barrier  $E_{\text{pd}}$  and particle binding energy  $E_b$  in Eq. (2.72) for a particle of type  $i$  as

$$E_{\text{pd}}^{(i)} = \sum_{j \in \mathcal{B}} n_j \Delta \varepsilon_{ij}, \quad (2.74)$$

$$E_{\text{b}}^{(i)} = \sum_{j \in \mathcal{B}} l_j \varepsilon_{ij} + \sigma \left( \sum_{j \in \mathcal{B}^*} n_j \right) \Delta \mu_i, \quad (2.75)$$

where  $\Delta \varepsilon_{ij}$  and  $\varepsilon_{ij}$  are, respectively, the peripheral diffusion energy and the binding energy specific for a pair of particles of types  $i$  and  $j$ . The function  $\sigma(x)$  is defined as follows:

$$\sigma(x) = \begin{cases} 1, & \text{if } x = 0 \\ 0, & \text{otherwise} \end{cases}. \quad (2.76)$$

The value  $\sigma = 1$  corresponds to the case when a particle detaches completely from its neighbours upon transition, whereas  $\sigma = 0$  stands for the case when at least one of its neighbours is preserved. Complete detachment of a particle from a group of other particles results in a change of chemical potential  $\Delta \mu_i$  specific for a particle of type  $i$ , and arises due to the entropy change in the course of particle detachment [152–156]. Note, that only mobile particles of the system impact the contribution to  $E_{\text{b}}^{(i)}$  arising due to the change of chemical potential, and therefore summation in the argument of function  $\sigma$  in Eq. (2.76) is performed over particle types  $\mathcal{B}^* \subseteq \mathcal{B}$ .

The peripheral diffusion energies  $\Delta \varepsilon_{ij}$ , determining the interaction between particles, could be deduced from the surface diffusion energy barrier. The binding energies  $\varepsilon_{ij}$  could be obtained once two particles of types  $i$  and  $j$  detach from each other. In a more general case, transition rates are constructed for all combinations of particle types and include binding energies  $\varepsilon$ , diffusion energy barriers  $\Delta \varepsilon$ , and chemical potential changes  $\Delta \mu$ .

### 2.5.4 Irradiation Driven Molecular Dynamics

Irradiation induced local quantum perturbations of a molecular system typically occur on the sub-femtosecond time scale and involve only those atoms that are directly affected by the irradiation. This results in the creation of secondary electrons, ions, reactive species (radicals), and excited molecules, which can further interact with the molecular system and cause further chemical transformations. This complex local dynamics typically involves the nearest environment of the targeted molecular site, being a small part of the entire molecular system, and is completed within femtoseconds. Within this interval some of the initial perturbations of the system, such as quasi-free electrons, electron holes, ionic charges, relax and vanish, due to the high electronic mobility and the Coulomb attraction. The femtosecond time scale is, however, still significantly shorter than the characteristic timescales responsible for the motion of the entire molecular system. Indeed, in classical MD a typical

integration time step is 1–2 fs, corresponding to the oscillation period of a hydrogen atom at room temperature.

The notable outcome of the process described above will be the emergence of bond breaks in the system. These events are most significant as they affect the dynamical behaviour and chemical transformations in the molecular system on the larger time scales, up to nanoseconds and beyond, being the typical time frame for the classical MD. The bond breaks arise in those parts of the molecular system which are targeted by the irradiation. They occur randomly with a probability depending on the intensity and the modality of irradiation. The probabilities of these events are related to the cross sections of the involved irradiation induced processes (elastic and inelastic scattering, electronic and vibrational excitation, dissociative electron attachment, collision dissociation, etc.) occurring in the system on the femtosecond time scale and can be elaborated from the collision theory or be taken from experiment.

Irradiation conditions of a molecular system can differ substantially and depend on the radiation modality, duration of the system exposure to irradiation and the system geometry. Irradiation can be a swift single event, like a single ion track crossing the molecular system, or it can last a certain period of time up to some nanoseconds and even longer. In the latter case the irradiation induced bond breaks and charge redistribution in the system occurs during the entire irradiation period. Irradiation can be homogeneous within a certain volume or strongly inhomogeneous. The choice of the irradiation conditions corresponds to each particular case study.

Hence, the Irradiation Driven Molecular Dynamics (IDMD) [16] can be introduced as classical MD with the superimposed random process of molecular bond breakage related to the irradiation conditions. The bond breakage is defined as the local alteration of the system force fields, which involves (i) creation of reactive atomic species (radicals) with dangling bonds, (ii) the possibility of dangling bonds' closure and creation of new molecular bonds or molecules, (iii) accounting for molecular topology changes (in the cases when it is defined, e.g. molecular mechanics force fields). The characterisation of these modifications of the classical MD force fields can be elaborated on the basis of quantum chemistry methods.

The proposed methodology aims to account for the major dissociative transformations of the molecular system induced by irradiation and possible paths of further reactive transformations. The latter are sensitive to statistical mechanical factors, like the concentration of the reactive species, their mobility (diffusion), the temperature of the medium, etc. All these factors are automatically accounted for in a correct way through the Langevin MD describing the molecular system as a NVT statistical mechanics ensemble. The local deviations from the statistical mechanics equilibrium arising in the vicinity of the breaking bonds caused by the local deposition of energy into the system leads to minor perturbations of the large molecular system and can be incorporated into IDMD as a perturbation.

The concept of IDMD introduced recently in [16] is general and applicable to any kind of molecular system treated with any type of classical force field. The method is implemented in MBN EXPLORER can operate with the large library of force fields implemented in the package. In its current realization IDMD is capable to describe systems modeled through pairwise potentials, many-body force fields, molecular

mechanics force fields (including the recently implemented reactive CHARMM force field [61], see Sect. 2.4) and their combinations. The limited number of parameters that determine molecular force fields, and their irradiation driven perturbations, results in a countable number of modifications that could occur in a molecular system upon irradiation and makes the method efficient and accurate. This implementation opens a broad range of possibilities for modelling of irradiation driven modifications and chemistry of complex molecular systems.

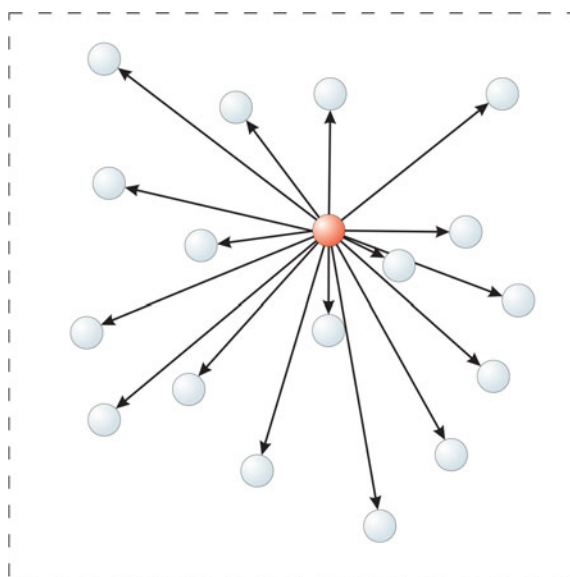
To highlight these possibilities, in Chap. 10 we present a case study of the FEBID process simulated by means of IDMD [16].

## 2.6 Computational Aspects of Multi-particle Simulations

### 2.6.1 Basic Interaction Approach

In the course of MD simulations it is necessary to recalculate forces which act on all particles in the system at every integration step of the simulation. The procedure can be rather computer time demanding for large molecular systems. For example, in the case of pairwise potentials each particle in the system interacts with all other particles (see Fig. 2.14). Thus, the calculation of all forces acting on the particles in the system requires the program to evaluate distances between all pairs of particles.

**Fig. 2.14** In the basic interaction scheme each particle of the system interacts with all other particles. The boundaries of the simulation box are shown by a *dashed line*



To implement the basic interaction scheme, the following procedure is introduced in MBN EXPLORER:

1. A static list of all interacting particles in the system is created prior to the first integration step.
2. For each particle from the created list, the algorithm determines an additional list of particles which interact with it.
3. For each particle in the system the forces acting on it are determined from the potential specified by the user.
4. The displacement of all particles in the system is performed according to their equations of motion with account for the evaluated forces.

In most of the cases the calculation of distances becomes the most computationally expensive part of the simulation. Therefore, the time needed to recalculate the interparticle distances defines the time,  $\tau$ , required for the whole simulation. For pairwise potentials,  $\tau$  is proportional to the squared number of particles,  $N^2$ , in the system. For many-body potentials (such as the Brenner or the Tersoff potentials), the simulation times increases even faster with the system size being proportional to  $N^3$ . Hence, the basic interaction approach, which accounts for all interactions in a molecular system, becomes extremely computationally expensive to perform long MD simulations for large systems (with  $N$  exceeding several thousands of atoms). The method should be only used for relatively small systems.

However, it is often possible to reduce significantly the number of interactions in the system if one neglects interactions between distant particles, or accounts for these distant interactions using certain “effective” potentials. Several algorithms which do so, and which are implemented in MBN EXPLORER are discussed below.

## 2.6.2 *Linked Cell Interaction Approach*

The general purpose of the linked-cell method for treating the interatomic interactions is to account for only the interactions between particles which are located not further than a user-specified separation distance,  $r_{\text{cut}}$ , called the “cutoff” radius, see Fig. 2.15a. For short-range interactions<sup>1</sup>  $r_{\text{cut}}$  can be defined as a distance beyond which the interaction of a particle with its neighbours is small enough to be neglected.

The linked-cell algorithm allows one to reduce significantly the computational time required for recalculating distances between particles in the system. The computational gain is achieved through constructing the lists of neighbour particles during several integration steps of a simulation. In general case, the neighbour list algorithm is faster than the method which accounts for all interactions in the system by a constant factor, but for several many-body potentials (such as the Brenner or/and the Tersoff potentials) the algorithm leads to the reduction of the computational cost from  $\mathcal{O}(N^3)$  to  $\mathcal{O}(N^2)$ . The neighbour list algorithm requires the mutual distances

---

<sup>1</sup>i.e. those which decrease faster than  $r^{-1}$ .

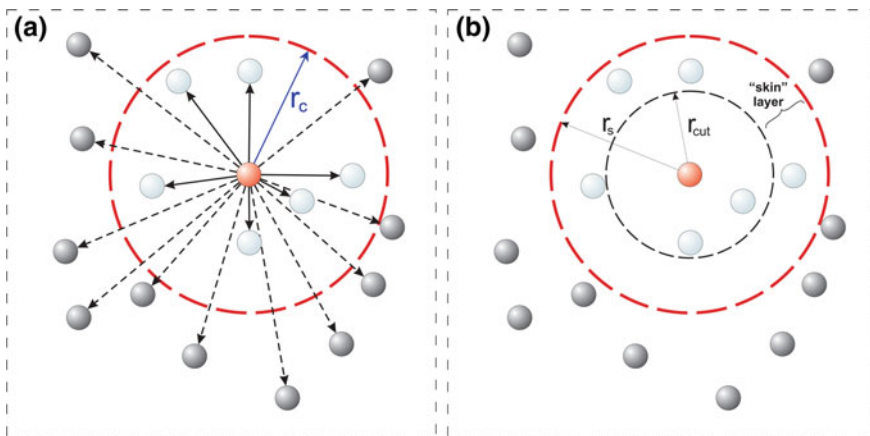


**Fig. 2.15** The scheme explaining how interactions in a system are treated using the neighbour list algorithm: **a** the central particle interacts only with particles that are located within a sphere of a radius  $r_c$  around it; **b** shows the definitions of the cutoff radius  $r_{cut}$ , the skin layer and the radius of the pair-list distance  $r_s$ . The boundaries of the simulation box are shown by dashed lines

between every pair of particles to be recalculated periodically. The recalculation is the most time demanding part of the calculations. To improve the computational cost further, more sophisticated numerical algorithms are necessary. Linked cell algorithm, implemented in MBN EXPLORER, allows to speed-up substantially the procedure treating the neighbour particles in the system.

The principal idea of the linked cell algorithm is to subdivide the simulation box into equal cubic cells, see Fig. 2.16. The cells form a three-dimensional lattice, and each cell is characterised by three integer numbers which define the cell Cartesian coordinates in the coordinate frame used in the simulation. Once the cells are defined, it is possible to assign the particles to cells, and to store this list in memory. The structuring of particles allows to reduce the number of computational operations in the following way. As already mentioned, the calculation of forces and potential energies in the system can be speed up by excluding the interactions between distant particles in the system. An important parameter which limits the range of the interactions is the cutoff distance. If the cutoff distance of potential is chosen equal or less than the cell size, then the particles located in a certain cell interact only with the particles in the neighbour cells. In a three-dimensional case each non-boundary cell has 26 neighbour cells.

To estimate the computational gain of the linked cell algorithm let us denote the average number of particles in a cell as  $N_c$ . Thus, for each cell it is necessary to evaluate  $N_c^2$  interparticle distances and  $27N_c^2$  distances for each cell with 26 neighbours. The total number of computational operations for the entire system is proportional to  $M^3 N_c^2$ , where  $M$  denotes the number of cells in each direction of the simulation box. Since the total number of particles in the system,  $N$ , is defined as



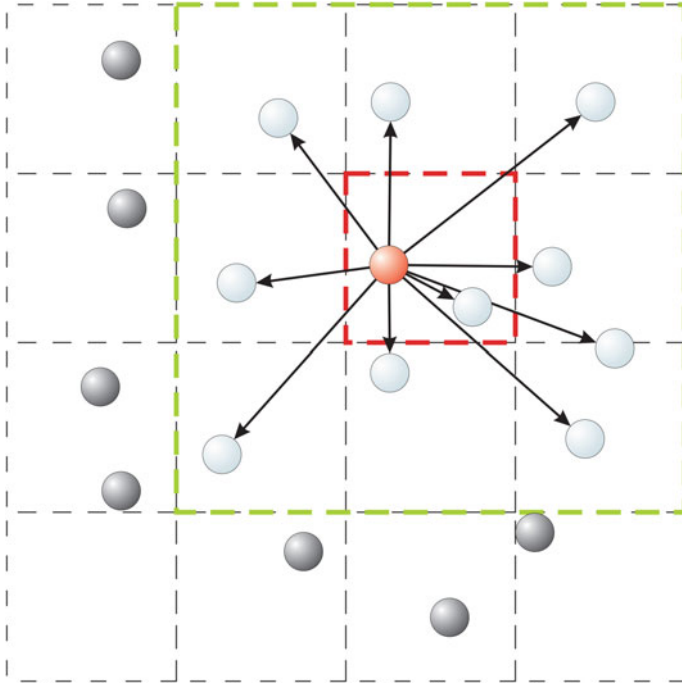


**Fig. 2.16** The linked cell algorithm splits the simulation box into equal cubic cells of a smaller size. The boundaries of the cells are shown by *dashed lines*. Each particle in the system interacts only with the particles which belong either to the same cell (shown with *red dashed lines*) or to the neighbour cells (*green dashed line*). All other particles (*dark gray circles*) are considered to be too distant and, therefore, do not contribute to the interaction in the system. The figure is adapted from [2]

$$N = M^3 N_c, \quad (2.77)$$

the total number of computational operations can be estimated as the product  $\sim N N_c$ . Thus, the computational efficiency of the linked cell algorithm is  $\mathcal{O}(N)$ , i.e. the computational cost scales linearly with the number of particles.

Figure 2.16 shows a mesh introduced in the simulation box, which subdivides it into equal cells. A particle denoted by the red color interacts with the light-blue particles located in the same cell and in the neighbour cells. All the interactions of the red particle which are to be accounted for, are shown by solid black arrows.

The following procedure is introduced in MBN EXPLORER in order to implement the linked cell algorithm:

1. The simulation box is split into cubic cells of equal size.
2. For each cell in the system the list of particles located in the current cell is created.

3. For each particle in a cell the interacting particles are determined. Two particles interact with each other if they are located in the same cell or in the neighbour cells.
4. The forces acting on the interacting particle's are evaluated according to the specified potentials. The equations of particles motion are integrated in time for one or several steps.
5. The assignment of particles to cells is updated.

Another big advantage of the linked cell algorithm is the straightforward implementation of periodic boundary conditions for the description of interactions in the system. It can be done by assigning the cells on one boundary of the simulation box as the neighbour cells for the cells on the other boundary. Periodic boundary conditions (described below in Sect. 2.6.3.2) allow one to avoid the border effects in the simulations and to treat the system as being infinite in all directions.

### 2.6.3 Boundary Conditions

Many computational tasks require to restrict the simulation space in order to avoid an unlimited expansion of the system. For this purpose it is necessary to specify the borders of the simulation space and to define the behavior of particles at the borders, i.e. to impose boundary conditions (BC). MBN EXPLORER includes BC of the two types: the reflective and the periodic BC.

#### 2.6.3.1 Reflective Boundary Conditions

Under the reflective BC, a particle colliding with the border of the simulation box is reflected back into the simulation volume. The reflection is treated as an elastic collision of the particle with a “virtual” infinitely heavy wall at rest. Thus, such collisions conserve the total energy of the system.

One should distinguish between the collision of a point-like particle and that of a rigid object with the wall.

A point-like particle has three degrees of freedom. Thus, its collision with the wall does not change the tangential component of the particle's velocity (momenta),  $\mathbf{v}_t$  but changes the sign of the normal component,  $v_n$ , of the velocity (momentum), as illustrated in Fig. 2.17. Written formally, this statment reads as follows:

$$\mathbf{v}'_t = \mathbf{v}_t, \quad v'_n = -v_n \quad (2.78)$$

where the primes mark the velocities after the collision.

Algorithmic implementation of the reflective RC for point-like particles is relatively simple. At each integration step, the program checks whether all particles in the system are going to be located inside the simulation box. In case of crossing

**Fig. 2.17** Under the reflective BC, a point-like particle with three degrees of freedom reflects elastically from a border of the simulation box. Here,  $\mathbf{v}$  and  $\mathbf{v}'$  are the particle's velocity before and after the collision,  $\mathbf{n}$  is the normal vector perpendicular to the border surface of at the collision point

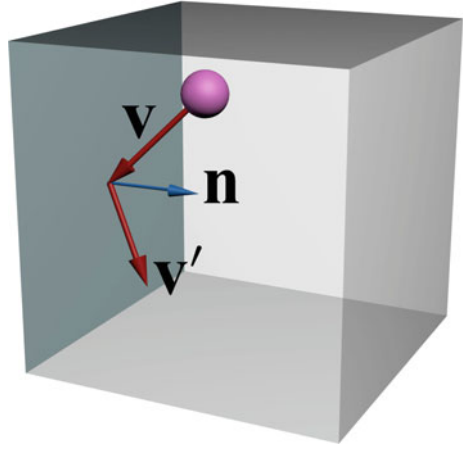
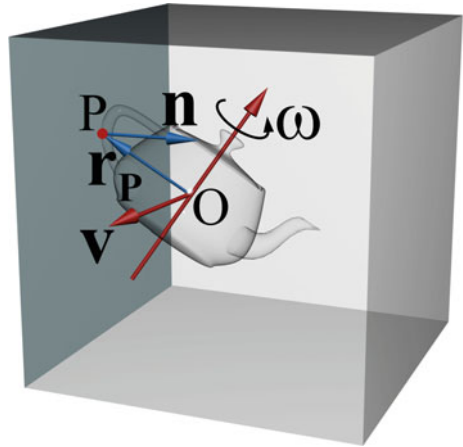


**Fig. 2.18** Elastic collision of a rigid molecular object with the simulation box boundary. The touch point is marked as  $P$ , the point  $O$  denotes the object's center-of-mass,  $\mathbf{r}_P$  stands for the vector  $\overrightarrow{OP}$ . The vectors  $\mathbf{n}$ ,  $\mathbf{v}$  and  $\boldsymbol{\omega}$  denote, respectively, the normal at  $P$ , the linear and angular velocities of the object before the collision



the box boundaries by a particle the program determines which boundary is to be crossed and then carries out the transformation of the particle velocity in accordance with Eq. (2.78).

In MBN EXPLORER, the reflective BC are also applied to rigid molecular objects characterised by six degrees of freedom. In this case, the object's center-of-mass velocity,  $\mathbf{v}'_{\text{CM}}$ , and angular velocity,  $\boldsymbol{\omega}'$ , after the elastic collision with the simulation box boundary are given by [2, 157]

$$\mathbf{v}'_{\text{CM}} = \mathbf{v}_{\text{CM}} + j\mathbf{n}M^{-1}, \quad \boldsymbol{\omega}' = \boldsymbol{\omega} + j\hat{I}^{-1}[\mathbf{r}_P \times \mathbf{n}]. \quad (2.79)$$

Here,  $\mathbf{v}_{\text{CM}}$  and  $\boldsymbol{\omega}$  are the velocities before the collision,  $\mathbf{n}$  is the normal at the touch point and  $\mathbf{r}_P$  denotes the position vector of the touch point with respect to the center-of-mass, see the illustrative Fig. 2.18. The quantity  $M$  is the mass of the rigid object

and  $\hat{I}^{-1}$  is its inverse inertia tensor. The so-called collision momentum  $j$  is defined as follows [157–159]:

$$j = -\frac{2(\mathbf{v}_{\text{CM}} + \boldsymbol{\omega} \times \mathbf{r}_p) \cdot \mathbf{n}}{M^{-1} + \hat{I}^{-1} [[\mathbf{r}_p \times \mathbf{n}] \times \mathbf{r}_p] \cdot \mathbf{n}}. \quad (2.80)$$

The following procedure is used to introduce reflections of a rigid molecular object:

1. At every simulation step the program checks if all particles constituting the rigid molecular object are within the simulation box.
2. If at a certain simulation step a particle is found outside of the simulation box, then the coordinates of this particle are taken as those of the touch point, and the vectors  $\mathbf{n}$  and  $\mathbf{r}_p$  are determined in the fixed laboratory coordinate frame.
3. If several particles of the rigid object simultaneously cross the border of the simulation box, the coordinates of these particles are averaged, and the resulting geometric mid-point is considered as the touch point.
4. Using the quaternion,  $\mathbf{Q}$ , assigned to the rigid object, the vectors  $\mathbf{n}$  and  $\mathbf{r}_p$  are transformed to the rigid object intrinsic coordinate frame (the object-frame) as follows:

$$\mathbf{n}^{(o)} = \overline{\mathbf{Q}} \circ \mathbf{n}^{(w)} \circ \mathbf{Q}, \quad \mathbf{r}_p^{(o)} = \overline{\mathbf{Q}} \circ \mathbf{r}_p^{(w)} \circ \mathbf{Q}, \quad (2.81)$$

where the superscripts  $(o)$  and  $(w)$  indicate the object and the laboratory frames, respectively. The symbol  $\circ$  denotes the quaternion multiplication by a vector [160].

5. A supplementary vector is defined, which is used to calculate the collision momentum

$$\mathbf{a} = \hat{I}^{-1}(\mathbf{r}_p^{(o)} \times \mathbf{n}^{(o)}), \quad (2.82)$$

The tensor  $\hat{I}^{-1}$  is diagonal in the rigid object intrinsic coordinate frame, so that  $\hat{I}_{ii}^{-1} = 1/\hat{I}_{ii}$ . Therefore, the calculation of  $\mathbf{a}$  in this frame is more efficient than in the laboratory frame.

6. The vector  $\mathbf{a}$  is recalculated in the laboratory frame:

$$\mathbf{a}^{(w)} = \mathbf{Q} \circ \mathbf{a} \circ \overline{\mathbf{Q}} \quad (2.83)$$

7. The collision momentum is calculated according to Eq. (2.80).
8. New values of the linear and angular velocities are calculated according to (2.79):

$$\mathbf{v}_{\text{CM}}'^{(w)} = \mathbf{v}_{\text{CM}}^{(w)} + j M^{-1} \mathbf{n}^{(w)} \quad (2.84)$$

$$\boldsymbol{\omega}'^{(w)} = \boldsymbol{\omega}^{(w)} + j \mathbf{a}^{(w)}. \quad (2.85)$$

Once the new linear and angular velocities are determined, the Euler-Newton equations of motion are further integrated as described in Sects. 2.2.1 and 2.2.3.

### 2.6.3.2 Periodic Boundary Conditions

Periodic BC provide an alternative way to treat particles in the vicinity of the simulation box boundaries. In contrast to the reflective BC, the periodic boundary conditions move the particles, approaching the boundary of the simulation box, to the opposite side of the simulation box. The magnitude and the direction of the particle's velocities do not change during this translation.

Thw Periodic BC provide an alternative way to treat particles in the vicinity of the simulation box boundaries. In contrast to the reflective boundary conditions, periodic BC constrain the motion of particles within the simulation box volume by translating particles exiting the simulation box from one side to its opposite side. The particles velocities are not affected by this translation.

The periodic BC replicate effectively the simulation box in all directions and allow one to avoid the surface effects in the system. The implementation of periodic BC in MBN EXPLORER implies that the particles being close to the boundary of the simulation box interact with “virtual” particles located on the other side of the boundary. The coordinates and atomic type names for the “virtual” particles are defined by real particles located on the opposite side of the simulation box. Figure 2.19 illustrates the principle of the periodic BC algorithm.

The periodic BC algorithm is implemented in MBN EXPLORER as follows:

1. The simulation box is split into cubic cells of equal size according.
2. For each cell in the system the list of particles located in the current cell is created.
3. For each cell the list of neighbour cells is determined. If a cell is located on a boundary of the simulation box, the cells located on the opposite side of the simulation box are also assigned as its neighbour cells.
4. For each particle in a cell the interacting particles are determined. Two particles interact with each other if they are located in the same cell or in the neighbour cells.
5. If a pair of particles is located in the two neighbouring cells located on the opposite sides of the simulation box, the distance between the particles is calculated as if one particle of the pair is located in a “virtual” cell on the other side of the simulation box boundary. Note that this “virtual” cell is located beyond the space of the simulation box.
6. The forces acting on the interacting particles are evaluated according to the specified potentials. The equations of motion are integrated in time for one or several steps.
7. The assignment of particles to the cells is updated.
8. If a certain particle leaves the simulation box, this particle is positioned in a cell on the opposite side of the simulation box. This procedure is performed by the shift of particle's coordinates on the length of the simulation box in the corresponding direction.

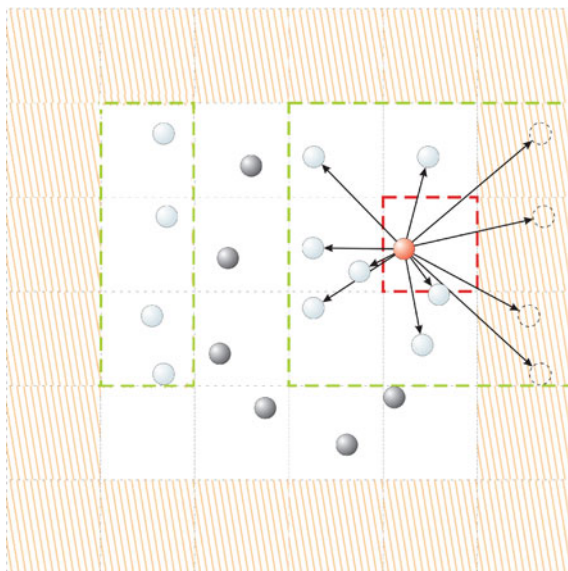


**Fig. 2.19** At the periodic BC the particles being close to the border of the simulation box interact with the “images” of particles from the opposite side of the simulation box. In this example, the *red* particle interacts with all *light-blue* particles located in the cells marked by the *dashed green line*

In order to use the periodic boundary conditions it is necessary to define the maximal distance for interparticle interaction, i.e. it is necessary to define the cutoff radius (see Fig. 2.15). An infinite cutoff radius leads to an infinite number of self-interactions of the particles in the system and, therefore, is pointless from computational and physical points of view. However, in the case of the long-range interactions such as the Coulomb interaction, it is not always possible to use a small cutoff radius without a considerable loss of accuracy of the simulation. In order to overcome these difficulties supplementary algorithms should be used (see e.g. the Ewald summation method discussed in Sect. 2.6.4.1 below). In MBN EXPLORER, the periodic BC require the use of the linked cell algorithm for treating the interatomic interactions. The size of a cell in this algorithm limits the long-range interactions and should be used carefully to ensure correct results of a simulation. A molecular system without long-range electrostatic interactions (e.g. without distant multiply-charged centers) is usually described fairly well using the linked cell algorithm with a reasonable cutoff.

### 2.6.4 Calculation of Coulomb Interactions

The simulation of the Coulomb interaction in the systems with periodic boundary conditions is not a trivial task. Due to the slow decrease of the potential with respect

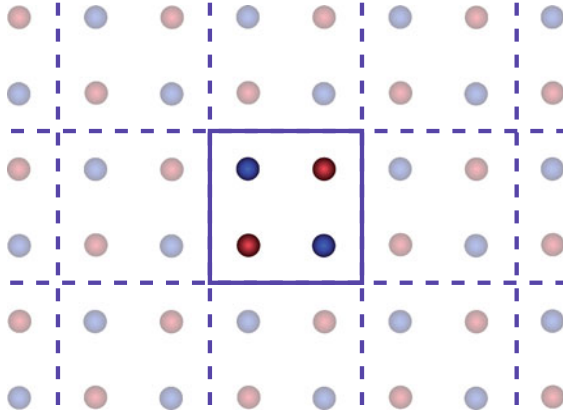


**Fig. 2.20** Infinite *cubic crystal* structure of point charges. Charges located within the simulation cell are shown by solid color, their images in other cells are shown as transparent

to distance the interaction of very distant atoms should be taken into account. Several methods were implemented in MBN EXPLORER to perform such calculations. A direct calculation of the Coulomb energy,  $U_C$ , of a periodic system (see, e.g., Fig. 2.20) can be performed according to the rule:

$$U_C = \frac{1}{2} \sum_{\mathbf{n}}^{\dagger} \sum_{i=1}^N \sum_{j=1}^N \frac{q_i q_j}{|\mathbf{r}_i - \mathbf{r}_j + \mathbf{n}|}, \quad (2.86)$$

where  $N$  denotes the total number of charged particles in the simulation cell,  $q_i$  is a charge of the  $i$ th particle,  $\mathbf{n} = (k, l, m)$  is a vector with integer components numerating periodic cells. The daggered summation indicates that the term with  $i = j$  is excluded when  $\mathbf{n} = 0$ .

In the case of pairwise calculation method the cutoff radius for long range Coulomb interactions has to be specified. The value of this parameter typically exceeds the size of the simulation box. In this case a number of images of the system will be generated as illustrated in Fig. 2.20. In each direction, the number of images is calculated by dividing the long range cutoff by the size of the simulation box in particular direction. For the generated system with limited number of images within the long range cutoff radius the summation written in Eq. (2.86) is carried out.

### 2.6.4.1 Ewald Summation for Long Range Interactions

Initially, the Ewald summation method was introduced to calculate the yield electrostatic energy of the periodic crystal lattices [161]. Later, it was adapted to calculate electrostatic forces in the non-crystalline systems with periodic boundary conditions [162].

The Ewald method comes to substitute a straightforward calculation of the Coulomb energy written in Eq. (2.86). The infinite sum in Eq. (2.86) is conditionally converged, depending strongly on the order of summation. The sum converges slowly, thus generally prohibiting its truncation after a certain term without violation of the computation accuracy.

The idea of the Ewald method is to screen each point charge of the system by a spherically symmetric charged cloud of the opposite charge so that the net charge of this new system equals to zero. In illustrative Fig. 2.21 the distributions of point charges is shown by vertical black lines, the charged clouds are shown by red peaked distributions. For each point charge, the cloud compensates its electric charge, therefore, the potential of the screened charge is a short-range one. As a result, the cumulative electrostatic potential of the whole system of screened charges can be calculated with desired tolerance. The electrostatic potential of the original system is then calculated as the difference between the cumulative potential in the modified system and the potential due to the charged clouds. The latter can be calculated using the Poisson summation formula, where the summation in real space is substituted by a summation of the Fourier transformed function in the reciprocal space:

$$\sum_{n=-\infty}^{\infty} f_n = \sum_{k=-\infty}^{\infty} \tilde{f}_k, \quad (2.87)$$

where  $\tilde{f}_k$  is the Fourier transform of  $f$ . Such calculation is only possible for the system with periodic BC.

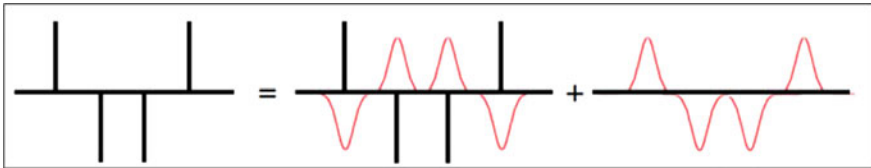


**Fig. 2.21** Illustration of the Ewald method. The compensating charge density (*red curve*) varies smoothly in space and is periodic. Therefore it can be approximated by a rapidly converging Fourier series



### 2.6.4.2 Ewald Summation Formula

The Coulomb potential  $1/r$  of a single particle of a unit charge can be written in the equivalent form:

$$\frac{1}{r} = \frac{1 - f(r)}{r} + \frac{f(r)}{r}, \quad (2.88)$$

where  $f(r)$  denotes the spatial distribution of the aforementioned cloud of the opposite charge. Usually, this function is considered in terms of the error function  $\text{erf}(x) = 2\pi^{-1/2} \int_0^x \exp(-t^2) dt$  representing a gaussian “cloud” with a so-called real/reciprocal space partition parameter  $\alpha$ :

$$f(r) = \text{erf}(\alpha r). \quad (2.89)$$

Using Eqs. (2.86)–(2.89) one writes the total electrostatic energy of the system as follows:

$$U_C = \frac{1}{2} \sum_{\mathbf{n}}^{\dagger} \sum_{i=1}^N \sum_{j=1}^N q_i q_j \left( \frac{\text{erfc}(\alpha |\mathbf{r}_{ij} + \mathbf{n}|)}{|\mathbf{r}_{ij} + \mathbf{n}|} + \frac{\text{erf}(\alpha |\mathbf{r}_{ij} + \mathbf{n}|)}{|\mathbf{r}_{ij} + \mathbf{n}|} \right), \quad (2.90)$$

where  $\mathbf{r}_{ij} = \mathbf{r}_i - \mathbf{r}_j$ , and  $\text{erfc}(x) = 1 - \text{erf}(x)$  stands for the complementary error function.

Applying the Poisson summation formula to the second term in Eq. (2.90), one derives the final expression for the electrostatic energy of the system with periodic boundary conditions:

$$\begin{aligned} U = & \underbrace{\frac{1}{2} \sum_{\mathbf{n}}^{\dagger} \sum_{i=1}^N \sum_{j=1}^N q_i q_j \frac{\text{erfc}(\alpha |\mathbf{r}_{ij} + \mathbf{n}|)}{|\mathbf{r}_{ij} + \mathbf{n}|}}_{\text{Real-space term}} \\ & + \underbrace{\frac{2\pi}{V} \sum_{|\mathbf{k}|>0} k^{-2} e^{-k^2/4\alpha^2} \left\{ \left| \sum_{i=1}^N q_i \cos(\mathbf{k} \cdot \mathbf{r}_i) \right|^2 + \left| \sum_{i=1}^N q_i \sin(\mathbf{k} \cdot \mathbf{r}_i) \right|^2 \right\}}_{\text{Reciprocal-space term}} \\ & - \underbrace{\frac{\alpha}{\sqrt{\pi}} \sum_{i=1}^N q_i^2}_{\text{Point self-energy}} - \underbrace{\frac{\pi}{2V\alpha^2} \left| \sum_{i=1}^N q_i \right|^2}_{\text{Charged system term}}. \end{aligned} \quad (2.91)$$

Here  $V$  is the volume of the simulation box,  $\mathbf{k}$  denotes the reciprocal lattice vector of periodic cells. The physical meaning of each term is noted below the corresponding summand.

### 2.6.4.3 Numerical Evaluation

For numerical applications it is necessary to truncate the summations in Eq. (2.91). In Ref. [163] the following cutoff values for the summations truncation are introduced:

- real-space cutoff,  $R_C$ : the real-space term includes only those real-space Coulomb pair interactions for which the distance between the particles is less than the cutoff distance:  $|\mathbf{r}_i + \mathbf{n}| < R_C$
- reciprocal-space cutoff,  $R_I$ , which constrains the value of the reciprocal-space lattice vector as:  $|\mathbf{k}| < R_I$ .

To minimize the computation time, the following values of the parameters  $\alpha$ ,  $R_C$  and  $R_I$  to obtain minimum calculation time were suggested [164]:

$$\alpha = \left( \frac{\pi^3 N t_R}{V^2 t_F} \right)^{\frac{1}{6}}, \quad R_C = \sqrt{\frac{-\log \varepsilon_E}{\alpha^2}}, \quad R_I = 2\alpha \sqrt{-\log \varepsilon_E}, \quad (2.92)$$

where  $\varepsilon_E$  is the *a-priori* estimate of the relative precision of energy,  $t_R$  and  $t_F$  are the execution times needed to evaluate a single term in the real and reciprocal space in Eq. (2.91), respectively [39]. The form of mathematical expressions for real and reciprocal space terms allows to propose, that computation times  $t_R$  and  $t_F$  should not differ significantly. Therefore, we assume that  $(t_R/t_F)^{1/6} \sim 1$  and neglect the corresponding multiplier in Eq. (2.92).

### 2.6.4.4 Fast Particle Mesh Ewald Summation Algorithm

Computational complexity of conventional Ewald summation algorithm discussed in the previous subsections scales as  $\mathcal{O}(N^2)$ , where  $N$  is the number of particles in the system. Therefore, the computational cost for evaluation of electrostatic interactions becomes prohibitive for larger systems. In order to overcome this limitation one has to employ an efficient way for calculating the reciprocal component of electrostatic energy, which can for example be achieved via the Fast Fourier Transformation (FFT) on a grid. One has to introduce a grid (or a mesh) that would subdivide the entire system and map charges in the system to the neighbouring mesh nodes. This operation scales linear with the number of particles, and, therefore, since FFT of the charge density to the reciprocal spaces has  $N \log N$  complexity, the computational cost of the entire procedure also scales as  $N \log N$ , allowing for computationally efficient treatment of larger systems. The method has historically been named as the Particle Mesh Ewald (PME) algorithm.

In MBN EXPLORER the so-called “Smooth particle particle mesh Ewald algorithm via cardinal B-Splines” is implemented. In this method cardinal B-Splines are used to map the charges to the mesh nodes. The details of the implemented algorithm can be found in Ref. [165]. Here we outline only the basic underlying ideas and in

the further notes we refer to the particular implementation of the algorithm in MBN EXPLORER as to PME method.

Similarly to the conventional Ewald algorithm, the PME method splits the calculation of the electrostatic energy between real and reciprocal spaces. Evaluation of the real-space contribution in PME is done exactly as in conventional Ewald, see the first and the last terms in Eq. (2.91).

Suppose there are  $N$  point charges  $q_1, q_2, \dots, q_N$  at positions  $\mathbf{r}_1, \mathbf{r}_2, \dots, \mathbf{r}_N$  within the MD simulation cell  $U$  satisfying  $q_1 + q_2 + \dots + q_N = 0$ . The orthogonal vectors  $\mathbf{a}_\alpha$ ,  $\alpha = 1, 2, 3$ , form the edges of the MD simulation unit cell. The conjugate reciprocal vectors  $\mathbf{a}_\alpha^*$  are defined via

$$\mathbf{a}_\alpha^* \cdot \mathbf{a}_\beta = \delta_{\alpha\beta}, \quad (2.93)$$

where  $\delta_{\alpha\beta}$  is the Kronecker symbol. The point charge  $q_i$  at position  $\mathbf{r}_i$  has fractional coordinates  $s_{\alpha i}$  defined by  $s_{\alpha i} = \mathbf{a}_\alpha^* \cdot \mathbf{r}_i$ . The charges interact according to the Coulomb's law, taking into account the periodic boundary conditions.

Let us define the reciprocal lattice vectors  $\mathbf{m}$  as

$$\mathbf{m} = m_1 \mathbf{a}_1^* + m_2 \mathbf{a}_2^* + m_3 \mathbf{a}_3^*, \quad (2.94)$$

where  $m_1, m_2, m_3$  are integers which do not turn zero simultaneously, and the structure factor  $S(\mathbf{m})$  by

$$S(\mathbf{m}) = \sum_{j=1}^N q_j \exp(2\pi i \mathbf{m} \cdot \mathbf{r}_j) = \sum_{j=1}^N q_j \exp[2\pi i (m_1 s_{1j} + m_2 s_{2j} + m_3 s_{3j})], \quad (2.95)$$

Then, the reciprocal term can be expressed in terms of the structure factors as follows:

$$E_{\text{rec}} = \frac{1}{2\pi V} \sum_{|\mathbf{m}| \neq 0} \frac{\exp(-\pi^2 \mathbf{m}^2 / \alpha^2)}{\mathbf{m}^2} S(\mathbf{m}) S(-\mathbf{m}), \quad (2.96)$$

where  $V = \mathbf{a}_1 \cdot (\mathbf{a}_2 \times \mathbf{a}_3)$  is the unit cell volume. The parameter  $\alpha$  is introduced in Eq. (2.89).

In order to approximate the electrostatic structure factors, we need to interpolate the complex exponentials appearing in Eq. (2.95). Given the positive integers  $K_1, K_2, K_3$  and a point  $\mathbf{r}$  in the unit cell, we denote its scaled fractional coordinates by  $u_1, u_2, u_3$ , i.e.,  $u_\alpha = K_\alpha \mathbf{a}_\alpha^* \cdot \mathbf{r}$ . Due to the periodic boundary conditions, we may assume that  $0 \leq u_\alpha < K_\alpha$ . Then

$$\exp(2\pi i \mathbf{m} \cdot \mathbf{r}) = \exp\left(2\pi i \frac{m_1 u_1}{K_1}\right) \exp\left(2\pi i \frac{m_2 u_2}{K_2}\right) \exp\left(2\pi i \frac{m_3 u_3}{K_3}\right). \quad (2.97)$$

Let us now define the cardinal B-Splines  $M_n(u)$  of the order  $n$ . For any real number  $u$ , the spline  $M_2(u)$  denotes the linear “hat” function given by  $M_2(u) = 1 - |u - 1|$  for  $0 \leq u \leq 2$  and  $M_2(u) = 0$  if otherwise. For  $n > 2$  the splines  $M_n(u)$  are generated by means of the recursion relation

$$M_n(u) = \frac{u}{n-1} M_{n-1}(u) + \frac{n-u}{n-1} M_{n-1}(u-1). \quad (2.98)$$

Then, the exponential functions from Eq. (2.97) can be written as follows:

$$\exp\left(2\pi i \frac{m_\alpha}{K_\alpha} u_\alpha\right) \approx b_\alpha(m_\alpha) \sum_{k=-\infty}^{\infty} M_n(u_\alpha - k) \exp\left(2\pi i \frac{m_\alpha}{K_\alpha} k\right) \quad (2.99)$$

with  $b_\alpha(m_\alpha)$  given by

$$b_\alpha(m_\alpha) = \exp\left(2\pi i (n-1) \frac{m_\alpha}{K_\alpha}\right) \left[ \sum_{k=0}^{n-2} M_n(k+1) \exp(2\pi i m_\alpha k / K_\alpha) \right]^{-1} \quad (2.100)$$

The error in the approximation, Eq. (2.99), is bounded from above by  $(2|m_\alpha|/K_\alpha)^n$ . The interpolation fails for  $n$  odd and  $2|m_\alpha| = K_\alpha$ , but since it occurs only in the tail of the reciprocal sum, one can set  $b_\alpha(m_\alpha)$  arbitrarily to zero in this case. Proceeding as above, the structure factor in Eq. (2.96) can be approximated by

$$\tilde{S}(\mathbf{m}) = b_1(m_1)b_2(m_2)b_3(m_3)F\left(Q(m_1, m_2, m_3)\right), \quad (2.101)$$

where  $F\left(Q(m_1, m_2, m_3)\right)$  denotes the discrete Fourier transform [165] of the array  $Q$  given by

$$Q(k_1, k_2, k_3) = \sum_{i=1}^N \sum_{n_1 n_2 n_3} q_i \prod_{\alpha=1}^3 M_n(u_{\alpha i} - k_\alpha - n_\alpha K_\alpha) \quad (2.102)$$

The approximate expression for the reciprocal term reads as follows [165]:

$$\begin{aligned} \tilde{E}_{\text{rec}} &= \frac{1}{2\pi V} \sum_{|\mathbf{m} \neq 0} \frac{\exp(-\pi^2 \mathbf{m}^2 / \alpha^2)}{\mathbf{m}^2} |b_1(m_1)|^2 |b_2(m_2)|^2 |b_3(m_3)|^2 \\ &\quad \times F\left(Q(m_1, m_2, m_3)\right) F\left(Q(-m_1, -m_2, -m_3)\right) \\ &= \frac{1}{2} \sum_{m_1=0}^{K_1-1} \sum_{m_2=0}^{K_2-1} \sum_{m_3=0}^{K_3-1} Q(m_1, m_2, m_3) (\mathcal{O}_{\text{rec}} \star Q)(m_1, m_2, m_3). \end{aligned} \quad (2.103)$$

Here  $\Theta_{rec} = F(B \cdot C)$  with  $C = \exp(-\pi^2 \mathbf{m}^2 / \alpha^2) / \pi V \mathbf{m}^2$ . The notation  $\Theta_{rec} \star Q$  denotes the convolution of  $\Theta_{rec}$  and  $Q$ .

To obtain the reciprocal component of the atomic force one differentiates right-hand side of Eq. (2.103) with respect to  $\mathbf{r}_i$ . The explicit final expression one finds in [165].

Multiscale Modeling of Complex Molecular Structure and  
Dynamics with MBN Explorer

Solovyov, I.A.; Korol, A.; Solov'yov, A.

2017, XV, 451 p. 209 illus., 202 illus. in color.,

Hardcover

ISBN: 978-3-319-56085-4